



**UNIVERSIDAD DE INVESTIGACIÓN DE  
TECNOLOGÍA EXPERIMENTAL YACHAY**

Escuela de Ciencias Químicas e Ingeniería

**Analogy between Chemical Kinetics and SIR/SEIR Models to  
evaluate the spread of Coronavirus Disease (COVID-19)  
contagion in Ecuador**

TRABAJO DE INTEGRACIÓN CURRICULAR PRESENTADO COMO  
REQUISITO PARA LA OBTENCIÓN DEL TÍTULO DE

QUÍMICO

**Autor:**

ANTONI VALENTIN PÁEZ LARA

**Tutor:** PH.D. FLORALBA LÓPEZ    **Co-Tutor:** PH.D SOLMAR VARELA

Urcuquí, Marzo, 2021

**SECRETARÍA GENERAL**  
**(Vicerrectorado Académico/Cancillería)**  
**ESCUELA DE CIENCIAS QUÍMICAS E INGENIERÍA**  
**CARRERA DE QUÍMICA**  
**ACTA DE DEFENSA No. UITEY-CHE-2021-00029-AD**

A los 5 días del mes de agosto de 2021, a las 15:30 horas, de manera virtual mediante videoconferencia, y ante el Tribunal Calificador, integrado por los docentes:

<b>Presidente Tribunal de Defensa</b>	Dra. PERALTA ARCIA, MAYRA ALEJANDRA DE JESUS , Ph.D.
<b>Miembro No Tutor</b>	Dr. TERCENIO THIBAUT , Ph.D.
<b>Tutor</b>	Dra. LOPEZ GONZALEZ, FLORALBA AGGENY , Ph.D.

El(la) señor(ita) estudiante **PAEZ LARA, ANTONI VALENTIN**, con cédula de identidad No. **1722293550**, de la **ESCUELA DE CIENCIAS QUÍMICAS E INGENIERÍA**, de la Carrera de **QUÍMICA**, aprobada por el Consejo de Educación Superior (CES), mediante Resolución **RPC-SO-39-No.456-2014**, realiza a través de videoconferencia, la sustentación de su trabajo de titulación denominado: **ANALOGY BETWEEN CHEMICAL KINETICS AND SIR / SEIR MODELS TO EVALUATE THE SPREAD OF CORONAVIRUS DISEASE (COVID-19) CONTAGION IN ECUADOR**, previa a la obtención del título de **QUÍMICO/A**.

El citado trabajo de titulación, fue debidamente aprobado por el(los) docente(s):

<b>Tutor</b>	Dra. LOPEZ GONZALEZ, FLORALBA AGGENY , Ph.D.
<b>Co - Tutor</b>	Dra. VARELA SALAZAR, SOLMAR ALEXANDRA , Ph.D.

Y recibió las observaciones de los otros miembros del Tribunal Calificador, las mismas que han sido incorporadas por el(la) estudiante.

Previamente cumplidos los requisitos legales y reglamentarios, el trabajo de titulación fue sustentado por el(la) estudiante y examinado por los miembros del Tribunal Calificador. Escuchada la sustentación del trabajo de titulación a través de videoconferencia, que integró la exposición de el(la) estudiante sobre el contenido de la misma y las preguntas formuladas por los miembros del Tribunal, se califica la sustentación del trabajo de titulación con las siguientes calificaciones:

Tipo	Docente	Calificación
Miembro Tribunal De Defensa	Dr. TERCENIO THIBAUT , Ph.D.	10,0
Tutor	Dra. LOPEZ GONZALEZ, FLORALBA AGGENY , Ph.D.	10,0
Presidente Tribunal De Defensa	Dra. PERALTA ARCIA, MAYRA ALEJANDRA DE JESUS , Ph.D.	10,0

Lo que da un promedio de: **10 (Diez punto Cero)**, sobre 10 (diez), equivalente a: **APROBADO**

Para constancia de lo actuado, firman los miembros del Tribunal Calificador, el/la estudiante y el/la secretario ad-hoc.

*Certifico que en cumplimiento del Decreto Ejecutivo 1017 de 16 de marzo de 2020, la defensa de trabajo de titulación (o examen de grado modalidad teórico práctica) se realizó vía virtual, por lo que las firmas de los miembros del Tribunal de Defensa de Grado, constan en forma digital.*

**PAEZ LARA, ANTONI VALENTIN**  
**Estudiante**

**Dra. PERALTA ARCIA, MAYRA ALEJANDRA DE JESUS , Ph.D.**  
**Presidente Tribunal de Defensa**

MAYRA ALEJANDRA DE JESUS PERALTA ARCIA  
 Digitally signed by MAYRA ALEJANDRA DE JESUS PERALTA ARCIA  
 Date: 2021.08.31 10:19:23 -05'00'

FLORALBA  
AGGENY LOPEZ  
GONZALEZ

Digitally signed by  
FLORALBA AGGENY  
LOPEZ GONZALEZ  
Date: 2021.08.31  
09:54:01 -05'00'

Dra. LOPEZ GONZALEZ, FLORALBA AGGENY , Ph.D.

**Tutor**

THIBAUT  
TERENCIO

Firmado digitalmente por THIBAUT  
TERENCIO  
DN: cn=THIBAUT TERENCIO o=EC I=QUITO  
ou=BANCO CENTRAL DEL ECUADOR,  
ou=ENTIDAD DE CERTIFICACION DE  
INFORMACION ECOSICE  
Materia: Soy el autor de este documento  
Ubicacion: Yachay/Tutor  
Fecha: 2021.08.30 12:59:45.00

Dr. TERENCIO THIBAUT , Ph.D.

**Miembro No Tutor**

CARLA SOFIA  
YASELGA NARANJO

Digitally signed by CARLA  
SOFIA YASELGA NARANJO  
Date: 2021.08.30 11:26:25  
-05'00'


YASELGA NARANJO, CARLA

**Secretario Ad-hoc**

## AUTORÍA

Yo, **Antoni Valentín Páez Lara**, con cédula de identidad 1722293550, declaro que las ideas, juicios, valoraciones, interpretaciones, consultas bibliográficas, definiciones y conceptualizaciones expuestas en el presente trabajo; así cómo, los procedimientos y herramientas utilizadas en la investigación, son de absoluta responsabilidad de el/la autora (a) del trabajo de integración curricular. Así mismo, me acojo a los reglamentos internos de la Universidad de Investigación de Tecnología Experimental Yachay.

Urcuquí, agosto 2021.



---

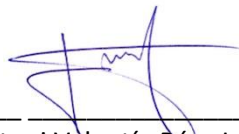
Antoni Valentín Páez Lara  
CI:1722293550

## AUTORIZACIÓN DE PUBLICACIÓN

Yo, **Antoni Valentín Páez Lara**, con cédula de identidad 1722293550, cedo a la Universidad de Tecnología Experimental Yachay, los derechos de publicación de la presente obra, sin que deba haber un reconocimiento económico por este concepto. Declaro además que el texto del presente trabajo de titulación no podrá ser cedido a ninguna empresa editorial para su publicación u otros fines, sin contar previamente con la autorización escrita de la Universidad.

Asimismo, autorizo a la Universidad que realice la digitalización y publicación de este trabajo de integración curricular en el repositorio virtual, de conformidad a lo dispuesto en el Art. 144 de la Ley Orgánica de Educación Superior

Urququí, agosto 2021.



---

Antoni Valentín Páez Lara  
CI:1722293550

*Dedicated to my family,  
for their unconditional love, comprehension and support.*

# Acknowledgments

This thesis represents the culmination of one of the essential hardness and thankfulness experiences of my life. First and foremost, I would like to thank god and my parents, Rodrigo and Judith, who have been my guidance and support throughout my life. To my brothers and sisters, Jhamel, Stefany, Alessandro Giancarlo, which constitutes my inspiration and support in all difficulties. Also, it is with immense gratitude that I acknowledge the support and help of my Professor Floralba López. I couldn't do this work without her knowledge and inspiration. Her way of seeing solutions to each problem is a great approach to define a genius. For me is a great pleasure to be one of her students. To my friends Bernardo, Alex, Sergio, Jorge, Patricio, and my partner Andrea, I support and stay with me in all of this journey. My eternal thanks to the School of Chemistry and engineering for guiding me through all my academic journey and awaken in me the passion and love for science. Finally, I would like to express my thanks to my university Yachay Tech. After years of effort, sacrifices, dedication, and joys, the day came when I would look back at the path traveled through your corridors and classrooms, and I would stop to thank you my alma mater.

# Resumen

El 13 de marzo de 2020, la OMS declaró una situación de emergencia pandémica global ocasionada por un nuevo coronavirus denominado SARS-CoV-2, posteriormente denominado COVID-19. En Ecuador la pandemia inicio en el mes de febrero con el primer caso detectado, rápidamente la pandemia colapso el sistema de salud y condenó a la sociedad ecuatoriana a un estado de crisis sanitaria. El siguiente trabajo propone implementar dos modelos epidemiológicos (SIR y SEIR) basados en los fundamentos del estudio del comportamiento cinético de las reacciones químicas, particularmente, reacciones cuadráticas u oscilantes fuera de equilibrio, las cuales, ocurren dentro de un reactor discontinuo y poseen una relación directa con el comportamiento de la dinámica de propagación del virus. Estas reacciones se encuentran representadas por un conjunto de ecuaciones diferenciales que permiten representar la tasa de cambio de cada una de las poblaciones de individuos consideradas en los modelos seleccionados. Posteriormente el modelo epidemiológico es utilizado para evaluar la dinámica de contagio de la pandemia en Ecuador utilizando datos recuperados de fuentes oficiales para distintos periodos establecidos. Finalmente, los resultados obtenidos muestran una aproximación cercana de la dinámica de propagación de la pandemia así como la eficiencia de las políticas de confinamiento lo que valida los modelos como herramientas de asistencia en la toma de decisiones.

**Keywords :** COVID-19, SIR, SEIR, Cinética Química.



# Abstract

On March 13, 2020, OMS declared a pandemic occasioned by a new coronavirus called SARS-CoV-2, also called COVID-19. This pandemic began to affect Ecuador in February of 2020, affecting the country's healthcare system and leaving profound affection to society. The following work proposes implementing two epidemiological models (SIR and SEIR) based on fundamentals of the kinetic study of chemical reactions. By considering the analogy of dynamics of the pandemic's spread with chemical reaction, particularly quadratic or oscillating reactions out of equilibrium occurring inside a batch reactor, the epidemiological model is implemented to evaluate the contagion dynamics of the pandemic in Ecuador. For this, a set of convenient differential equations allows representing the rate of change of each of the populations of individuals considered in selected models. The data used for the models were retrieved from official sources, and different periods were established. Finally, the results obtained show a close approximation of curfew policies' efficiency on pandemic dynamics that validate the models as secondary assessment tools.

**Keywords :** COVID-19, SIR, SEIR, Chemical Kinetics.

# Contents

<b>Acknowledgments</b>	<b>ii</b>
<b>Resumen</b>	<b>iii</b>
<b>Abstract</b>	<b>iv</b>
<b>1 Introduction</b>	<b>1</b>
<b>2 Chemical Kinetics overview: Complex Mechanism</b>	<b>4</b>
§2.1 Law of Mass Action . . . . .	6
§2.2 Steady State Approximation . . . . .	7
§2.3 Arrhenius equation . . . . .	10
§2.4 Transition State Theory . . . . .	13
§2.5 Oscillating Reactions . . . . .	14
<b>3 Mathematical Models in Epidemiology</b>	<b>20</b>
§3.1 The SIR dynamic model of infectious diseases . . . . .	23
§3.2 Basic Reproductive Ratio ( $R_0$ ) - Threshold Phenomena . . . . .	26
§3.3 The SEIR model: Adding a latent period to SIR model . . . . .	27
§3.4 SEIRD model: Modelling post death transmission . . . . .	29
<b>4 Novel Zoonotic Epidemic: COVID-19</b>	<b>33</b>
§4.1 Historical worldwide Zoonotics Epidemics . . . . .	33
§4.2 SARS-CoV-2: Pathogenesis and Characteristics . . . . .	34
§4.3 COVID-19 Pandemic . . . . .	36
<b>5 Problem Statement and Objectives</b>	<b>38</b>

§5.1 Problem Statement . . . . .	38
§5.2 Objectives . . . . .	39
§5.2.1 General Objective . . . . .	39
§5.2.2 Specific Objective . . . . .	39
<b>6 Methodology</b>	<b>40</b>
§6.1 The SIR and SEIR Analogy . . . . .	40
§6.1.1 Models description . . . . .	41
§6.1.2 Estimation of Transmission ( $\beta$ ) and recovery rate ( $\gamma$ ) . . . . .	43
<b>7 Results</b>	<b>46</b>
§7.1 Data Selection . . . . .	46
§7.2 Epidemiological Characteristics of Ecuador . . . . .	47
§7.2.1 Confirmed Cases and their incidence . . . . .	47
§7.2.2 Associated and confirmed fatalities related to COVID-19 . . . . .	49
§7.3 Forecasting COVID-19 epidemic dynamics through SIR and SEIR simulations.	53
§7.3.1 SIR MODEL . . . . .	53
§7.3.2 SIR model simulation for LD-0-1: $\beta = 0.44$ , $\gamma = 0.052$ , $R_0 = 8.79$	58
§7.3.3 SIR model simulation for LD-0-2: $\beta = 0.15$ , $\gamma = 0.052$ , $R_0 = 3.03$	60
§7.3.4 SIR model simulation for LD-0-3: $\beta = 0.12$ , $\gamma = 0.052$ , $R_0 = 2.43$	61
§7.3.5 SIR model simulation for CP-1: $\beta = 0.18$ , $\gamma = 0.052$ , $R_0 = 3.60$ .	62
§7.3.6 SIR model simulation for LD-2: $\beta = 0.12$ , $\gamma = 0.052$ , $R_0 = 2.40$ .	63
§7.3.7 SIR model simulation for LD-3: $\beta = 0.11$ , $\gamma = 0.052$ , $R_0 = 2.20$ .	64
§7.3.8 SEIR MODEL . . . . .	67
<b>8 Conclusions</b>	<b>70</b>

# List of Figures

2.1	Relation of chemical species concentration vs. time for different conditions of constant rates in chemical reactions involving intermediate species [12]. . . . .	9
2.2	Oscillatory behavior of intermediate concentrations from the Lotka-Volterra mechanism [12]. . . . .	17
2.3	Illustration of the dependence of the reaction rate on the coefficient of reaction advancement $\xi$ . Retrieved from [12]. . . . .	19
3.1	Representation of the time-line of infection, showing the dynamics of the pathogen (gray area) and the host immune response (black line) as well as labeling the various infection classes: susceptible, exposed, infectious, and recovered. Note that the diseased period, when symptoms are experienced, is not necessarily correlated with any particular infection class. Retrieved from [23]. . . . .	22
3.2	Schematic SIR flowchart. [23] . . . . .	24
3.3	Sample SIR chart with an initial conditions of $S(0) = 1000, I(0) = 1, R(0) = 2.5$ Population Fraction: 1/1000. The variance trough time of S,I and R is observed.	26
3.4	Estimated Basic Reproductive Ratios for different diseases. [23] . . . . .	27
3.5	SEIR Flowchart.[23] . . . . .	28
3.6	Schematic SEIRD Flowchart [37]. . . . .	30
3.7	SEIRD variation with asymptomatic individuals Flowchart [38]. . . . .	31
4.1	a) Schematic structure of the S protein of SARS-CoV-2.b) Protein-receptor (ACE2) interaction and c) Cell fusion process Retrieved from [45] . . . . .	34

4.2 Lung CT of a patient with COVID-19. (A) Peripheral mild ground glass opacity's in the left lower lobe (arrow). (B) Three weeks later, at the same lung zones, the disease has rapidly progressed and fibrotic changes are now evident (arrows). Retrieved from [52] . . . . . 35

4.3 Cumulative confirmed COVID-19 deaths per million people. Coronavirus Pandemic (COVID-19)". Retrieved from: 'https://ourworldindata.org/coronavirus'[57] 36

7.1 Daily variance of COVID-19 positive cases in Ecuador. Data Retrieved from online database: [6, 72, 73] . . . . . 48

7.2 Cumulative chart of positive reported cases to november 2020. Data retrieved from:[6, 72, 73] . . . . . 49

7.3 Cumulative daily confirmed and related deaths to COVID-19 disease. Data retrieved from online database: [6, 72, 73]. . . . . 50

7.4 Cumulative daily deaths confirmed and related to COVID-19 disease. Data retrieved from online database: [6, 72, 73] . . . . . 51

7.5 Historical Comparative Chart of cumulative deaths from March to November period. Data retrieved from online database: [6, 72, 73] . . . . . 52

7.6 Left: Linear regression of the function  $Ln(I)$  vs.  $t$  for the first three temporal partitions: LD-01 (A), LD-02 (C), LD-03 (E), from which the relation between kinetic parameters associated with COVID-19 epidemic are determined from the slope  $m$  estimated for each regression. Right: Recovery rate ( $\gamma$ ) as a function of the time for the first three temporal partitions: LD-01 (B), LD-02 (D), LD-03 (F). 55

7.7 Left: Linear regression of the function  $Ln(I)$  vs.  $t$  for the last three temporal partitions: CP-1 (A), LD-2 (C), LD-3 (E), from which the relation between kinetic parameters associated with COVID-19 epidemic are determined from the slope  $m$  estimated for each regression. Right: Recovery rate ( $\gamma$ ) as a function of the time for the last three temporal partitions: CP-1 (B), LD-2 (D), LD-3 (F). . 56

7.8 Variation of basic reproductive ratio ( $R_0$ ) through temporal periods considered. 57

7.9 Results for SIR model for temporal period LD-0-1:  $\beta=0.44$   $\gamma=0.052$  and  $R_0=8.79$ . Initial Ecuadorian susceptible population: 17,000,000 . . . . . 59

7.10 Results for SIR model for temporal period LD-0-2:  $\beta=0.15$   $\gamma=0.05$  and  $R_0=3.03$ .  
     Initial Ecuadorian susceptible population :16,999,465. . . . . 61

7.11 Results for SIR model for temporal period LD-0-3:  $\beta=0.12$   $\gamma=0.05$  and  $R_0=2.43$ .  
     Initial Ecuadorian susceptible population: 16,995,410. . . . . 62

7.12 Results for SIR model for temporal period CP-1:  $\beta=0.18$   $\gamma=0.052$  and  $R_0=3.60$ .  
     Initial Ecuadorian susceptible population: 16,995,410. . . . . 63

7.13 Results for SIR model for temporal period LD-2.  $\beta=0.12$   $\gamma=0.05$  and  $R_0=2.40$ .  
     Initial Ecuadorian susceptible population: 16,987,451. . . . . 64

7.14 Results for SIR model for temporal period LD-3.  $\beta=0.12$   $\gamma=0.05$  and  $R_0=2.20$ .  
     Initial Ecuadorian susceptible population: 16,955,386. . . . . 65

7.15 Comparative chart of COVID-19 infected curve peak from established periods . . . . . 66

7.16 SEIR model configuration values. . . . . 67

7.17 SEIR Chart.  $R_0=2.74$ . Probabilities: Hosp:0.21, ICU:0.05 Death:0.02. Ecuado-  
     rian Population Susceptible considered:17000000 . . . . . 68

7.18 Amplified curves of Susceptible, Exposed, Infected and Deaths related to SEIR  
     model . . . . . 69

# List of Tables

- 7.1 Temporal sections for different periods during COVID-19 epidemic based in the social management in Ecuador. . . . . 47
- 7.2 Estimation of transmission ( $\beta$ ) and recovery ( $\gamma$ ) rates and basic reproductive ratio ( $R_0$ ) determined by using retrieved data for COVID-19 in Ecuador. . . 54
- 7.3 Kinetic parameters associated to COVID-19 epidemic in Ecuador: transmission ( $\beta$ ) and average recovery ( $\gamma$ ) rates and re-normalized basic reproductive ratio ( $R_0$ ), determined by using official retrieved data reported in Ecuador. 58

# Chapter 1

## Introduction

The *Chemical Kinetics* is a field of chemistry that involves studying the rates and mechanisms involved in chemical reactions, for which collisions between molecules occur with specific energy depending on molecular orientation. The diffusion of the different species involved, as well as the strength of the interaction between them, conditions the rate at which the chemical reaction occurs, both processes being governed by the temperature. Chemical reactions exhibit different kinetic parameters that characterize them, representing their dependence with temperature and concentrations of reactants species, which are experimentally determined. In general, the analysis of the dependence with the concentration of species involved followed by an appropriate differential equations system representing the temporal evolution of these species during the reaction period. This analysis of the temporal evolution of chemical species has extended to the analysis of the spreading capacity of a pathogen in a group of individuals,<sup>1</sup> and it has even been the basis of predator-prey models, well known in biological topics.<sup>2</sup>

Some epidemiological models in which the changes in the individuals' healthiness due to the spread of infectious diseases are analyzed present conceptual analogies with the underlying fundamentals of Chemical Kinetics. From these models is allowed an evaluation of the epidemic dynamic, identifying the kinetic parameters associated with it, for example, the frequency at which the new cases are occurring, that is, the epidemic spreading. The rate of new positive cases produced by a specific epidemic with the human-human transmission can be modeled assuming that the encounters or collisions between an *in-*



*infected* individual and some who are not, called *susceptible* individuals, produce an increase in infectious individuals. Principally, these phenomena occur due to the lack of immunity against the disease, facilitating the disease's spread. The spread process occurs according to the intrinsic dynamic of the epidemic, whose kinetic parameter can be obtained through kinetic mechanisms proposed from the changes in the infected population,<sup>3</sup> and it can be controlled by the restrictive mobility measures of the population. After a characteristic period, a fraction of infected individuals become *recovered* individuals, which is dependent on some factors such as the immune system of individuals, accessibility of the population to hospital resources, and the policies involved in managing the epidemic.<sup>4</sup>

The first stage of an epidemic, related to the transfer of pathogen due to the encounters or collision between infected and susceptible individuals, occurs with a probability associated with the epidemic transmission, identified by the kinetic parameter termed as  $\beta$  in what follows. In the second stage, the infected individuals undergo two alternatives: they could recover or, unfortunately, die. The probability for each of these alternatives is related to individuals' immune system, hospital resources, and the public health system's policies. This probability is identified with other important kinetic parameters defined as  $\gamma$ . The epidemiological models proposed with the above-described stages are known as compartmental models SIR and SEIR,<sup>5</sup> whose acronyms are related to the identification of types of individuals:

$$S = \textit{Susceptible}$$
$$E = \textit{Exposed}$$
$$I = \textit{Infected}$$
$$R = \textit{Recovered}$$

Both models are based on the analysis of temporal evolution of each of these types of individuals, which is carried out by solving the differential equations system that results according to the analogy with the appropriate kinetic mechanism, being adjustable to the daily information of COVID-19 provided by the the Comité de Operaciones de Emergencia of Ecuador.<sup>6</sup> Both models allow us to obtain the kinetic parameters associated with the dynamic of the spread of the epidemic, taking into account that they are highly dependent on the data being accurate and reliable to generate continuous predictions about the later evolution of the epidemic.

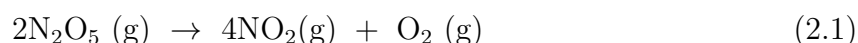
In this work, we propose implementing two epidemiological models based on fundamentals of the kinetic study of chemical reactions by considering the analogy of dynamics of the pandemic's spread, assuming the model of study to a batch reactor carrying out an autocatalytic reaction with catalyst deactivation. This model is based on a coupled ordinary differential equations (ODEs) that describe the temporal evolution of the spatially homogeneous mixture of chemically reacting species. Furthermore, due to its characteristics, the models can be defined as an analogy of the classic epidemiologic models: Susceptible - Infectious - Recovered (SIR) and Susceptible - Exposed - Infectious - Recovered (SEIR).

# Chapter 2

## Chemical Kinetics overview: Complex Mechanism

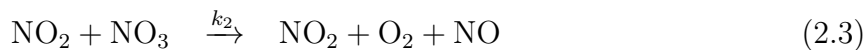
*Chemical Kinetics* is a chemistry field in which the collisions between molecules of different chemical species and their dynamics are studied. The different collisions between molecules may be defined as kinetic steps that allow the gather of chemical information. The set of individual kinetic processes that allows chemical reactants' transformation into chemical products is defined as reaction mechanisms. These mechanisms are commonly used as a guide to predict the rate law expression and, therefore, the order of that chemical reaction. On the other hand, they allow categorizing the type of chemical reaction according to the steps involved. In the case of a chemical reaction, which involves a single elementary step, the reaction mechanism is defined as a simple reaction, and, for two or more elementary steps, it is defined as a complex reaction.<sup>7</sup>

As an example, the decomposition reaction of dinitrogen pentoxide, given in the equation 2.1, could be reached by a single step consisting of a bi-molecular collision between two  $\text{N}_2\text{O}_5$  molecules, in whose case it would correspond to a simple reaction:



However, for a reaction mechanism to be valid, the rate-law expression predicted by the proposed mechanism must be corroborated experimentally.<sup>7</sup> In the case of 2.1, it is neces-

sary to reevaluate the mechanism and propose a new one consistent with the experimental results as follows:



In this proposed mechanism, the first step in 2.2 represents an equilibrium between the  $\text{N}_2\text{O}_5$  species to  $\text{NO}_2$  and  $\text{NO}_3$  species, which is defined by the rate constants  $k_1$  and  $k_{-1}$  for the forward and backward reactions of equilibrium, respectively. The number two besides  $\text{N}_2\text{O}_5$  species indicates the number of times that this step occurs in the reaction mechanism. In the second step illustrated in the reaction 2.3, the bi-molecular reaction of  $\text{NO}_2$  and  $\text{NO}_3$  species results in a separation of  $\text{NO}_3$  to product  $\text{NO}$  and  $\text{O}_2$ , having associated a rate constant  $k_2$ . Finally, the reaction given in 2.4,  $\text{NO}$  and  $\text{NO}_3$  species undergo a bi-molecular reaction to produce  $2\text{NO}_2$  whose rate constant is given by  $k_3$ . The stoichiometric numbers of a correct proposed mechanism must match the stoichiometric of the reaction.<sup>7</sup>

The previous mechanism suggests the formation of  $\text{NO}$  and  $\text{NO}_3$ , although these species are not considered reactants nor products of that reaction. However, their presence justifies the experimental results, and without them would be no possibility to do it. These species are produced and fully consumed during the proposed mechanism, and therefore they are chemical species denominated as reaction intermediates.<sup>7</sup>

As mentioned before, to verify the accuracy of the proposed mechanism of a chemical reaction, the rate law suggested must reproduce the one experimentally obtained for such reaction. It is needed to evaluate the chemical kinetics of that reaction, evaluating the reactants species' consumption rate or formation of product species during the course of the chemical reaction. The time-evolution analysis of each species implies defining *differential equations* by which the rate of consumption or/and production of these species are represented, and therefore the rate reaction is established.

Following with the reaction described before and by assuming the proposed mechanism

in 2.2 - 2.4 as valid, the rate of reaction ( $v_{rx}$ ) can be expressed by the consumption rate of the reactant species, that is:

$$v_{rx} = -\frac{1}{2} \frac{d[\text{N}_2\text{O}_5]}{dt} = k [\text{N}_2\text{O}_5]^2 . \quad (2.5)$$

In this equation, the rate law for such chemical reactions is related to the term  $k$ , which considers the temperature dependence, as well as the concentration of reactant species dependence, resulting in a second-order reaction for  $\text{N}_2\text{O}_5$ .<sup>7</sup>

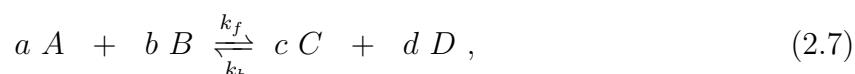
To obtain the rate law for a chemical reaction, by specifying the order of reaction for the reactant species, as well as the value for  $k$ , it is required to propose a mechanism and evaluate the time evolution of the involved species. According to the previously proposed mechanism for the decomposition reaction of  $\text{N}_2\text{O}_5$ , given in 2.2 - 2.4, the differential equation representing the time variation of the  $\text{N}_2\text{O}_5$  results in:

$$\frac{d[\text{N}_2\text{O}_5]}{dt} = -k_1[\text{N}_2\text{O}_5] + k_{-1}[\text{NO}_2][\text{NO}_3] \quad (2.6)$$

In general, the mechanism proposed is consistent with the experimentally obtained rate law proven otherwise, which requires evaluating different experimental conditions demonstrating that the reaction must occur by the sequential steps mechanism proposed.

## 2.1 Law of Mass Action

In 1864, Guldberg and Waage propose a statement to describe the chemical kinetics of a system at equilibrium.<sup>8,9</sup> The statement begins with the general reaction in which reactant species  $A$  and  $B$  react to give product species  $C$  and  $D$ , that is:



reflecting the balance of the rates of reactions in the forward and backward directions, for which the stoichiometric coefficient  $a$ ,  $b$ ,  $c$  and  $d$  have to be considered. The representation

of the rate of both reactions can be expressed as:

$$v_f = k_f [A]^a [B]^b \quad (2.8)$$

$$v_b = k_b [C]^c [D]^d, \quad (2.9)$$

and since the equilibrium of that reaction implies a balance of their rates,  $v_f = v_b$ , the equilibrium conditions imply:

$$k_f [A]_{eq}^a [B]_{eq}^b = k_b [C]_{eq}^c [D]_{eq}^d. \quad (2.10)$$

The statement of Goldberg and Waage proposes that if at a given temperature (T) a chemical system is at equilibrium, then the ratio of the rate constants becomes a constant, which is denoted by  $K_{eq}$  and whose expression obtained from 2.10 results in:

$$K_{eq}(T) = \frac{k_f}{k_b} = \frac{[C]_{eq}^c [D]_{eq}^d}{[A]_{eq}^a [B]_{eq}^b}. \quad (2.11)$$

As it is perceived, equation 2.11 considers the concentrations of chemical species involved in the reaction and, as a consequence, the rate of an elementary reaction is equal to the product of the concentration of the reactants.<sup>10</sup> In the case of uni-molecular reactions, the reaction rates increase linearly with the reactant's concentration and are related to the probability of collision between species involved in a fixed time interval. For the case of bi-molecular reactions, the probability of collision increases due to that it is directly related to the amount of concentration.<sup>10,11</sup>

## 2.2 Steady State Approximation

In some mechanisms of reactions, one or more intermediate species are involved, which are frequently very reactive species, so that their accumulation to any significant amount could be not reached during the reaction. The following equations represent an example

of such mechanism:



where are indicated the rate constants  $k_x$  for each step, and the intermediate reaction is represented by the specie  $I$ . The set of differential rate expressions for each species associated with such mechanism corresponds to:

$$\frac{d[A]}{dt} = -k_1 [A] \quad (2.14)$$

$$\frac{d[I]}{dt} = k_1 [A] - k_2 [I] \quad (2.15)$$

$$\frac{d[P]}{dt} = k_2 [I]. \quad (2.16)$$

How the concentration of intermediate species evolves during the reaction course depends on the speed of the different steps involved in the mechanism, that is, of the relative magnitudes of the rate constants  $k_1$ , and  $k_2$ . For the illustrated example, if the first step is faster than the second one, that is,  $k_1 > k_2$ , the intermediate species concentration changes markedly during the reaction, increasing and then decreasing at the end of the reaction, as is showed in figure 2.1-a. The greater the  $k_1$  compared to  $k_2$ , the greater the maximum value of the intermediate species' concentration, and it will appear at times closer to the beginning of the reaction.

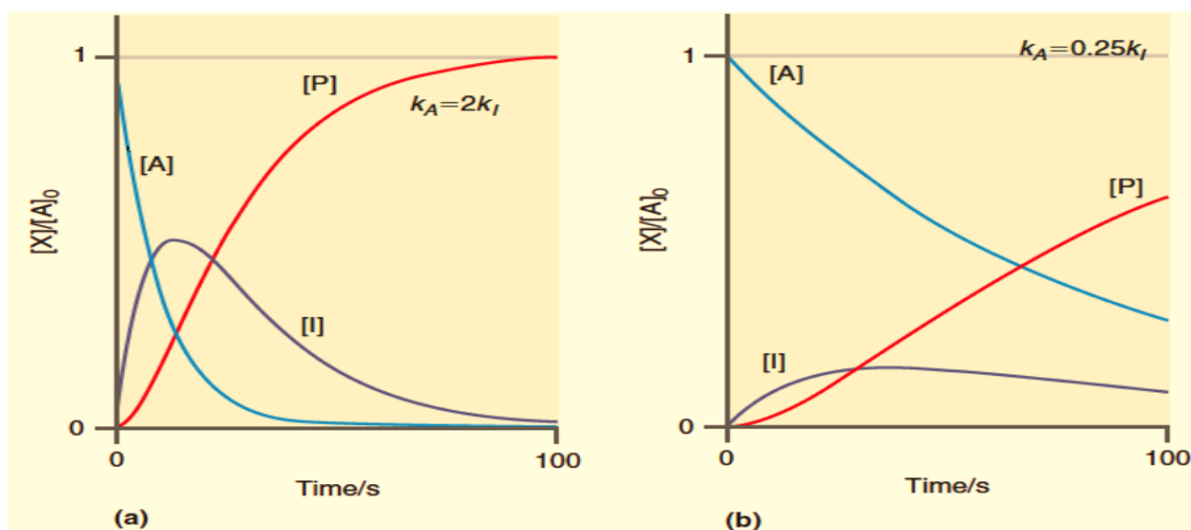


Figure 2.1: Relation of chemical species concentration vs. time for different conditions of constant rates in chemical reactions involving intermediate species [12].

In contrast, if the second reaction step associated with the rate constant  $k_2$  is faster than the first step with  $k_1$ , the concentration of  $[I]$  will be quite small, that it is even difficult to detect. This limit, represented in figure 2.1-b, applies for the most reactions, in which it is considered that an accumulation of species  $I$  does not occur. From this, it can be established the following relation between the involved species:

$$[I] \ll [A] \quad (2.17)$$

$$[I] \ll [P] ,$$

indicating the low concentration of intermediate species compared to the concentration of the reactant and product species. That situation assumes that  $[I]$  builds up quickly to this small concentration that remains relatively constant during the reaction, that is:

$$\frac{d[I]}{dt} = 0 . \quad (2.18)$$

The equation 2.18 represents the steady-state approximation, occasionally called the stationary-state or *Bodenstein's Quasi-Steady State Approximation*,<sup>13</sup> which involves setting the rate of change of a reaction intermediate in a reaction mechanism equal to zero



so, the kinetic equations can be expressed as a function of the concentrations of chemical species in macroscopic amounts. It is convenient to mention that, based on the principle of conservation of mass applied to previous equations considering a constant volume, the concentration of the chemical species at any stage of reaction are connected by:

$$[A] + [I] + [P] = [A]_0 \quad (2.19)$$

where  $[A]_0$  represents the initial concentration of the reactive species, which is a constant. Using the steady state approximation, the equation 2.19 results in:

$$\frac{d[P]}{dt} = - \frac{d[A]}{dt} \quad (2.20)$$

showing that the rate of formation of  $[P]$  is equal to the rate of disappearance of  $[A]$ .

## 2.3 Arrhenius equation

In the late 1800s, the physicist Svante August Arrhenius proposed an empirical expression based on the relationship between the rate constant of a chemical reaction and the temperature at which it is carried out.<sup>14</sup> From his experiments, Arrhenius realized that, for many reactions, a linear behavior, or close to it, is observed when evaluating the temperature dependence of rate constants by the function  $\ln(k)$  versus  $T^{-1}$ . From this statement, the equation suggested for that dependence, known as the *Arrhenius equation*, is:

$$k = A_Z e^{\frac{-E_a}{RT}} , \quad (2.21)$$

Where  $E_a$  refers to the activation energy, that is, the minimum value that the energy involved in molecular collisions must reach in order to be effective and produce a chemical reaction. The units of  $E_a$  are the same as those for  $RT$ . The term  $A_Z$  refers to the *pre-exponential factor* or *Arrhenius factor*, and its units are the same as those of  $k$ . The Arrhenius equation's initial proposal implies that the terms  $E_a$  and  $A_Z$  are constant values without a temperature dependence. Nevertheless, a more sophisticated approach has led

to an equation similar to the Arrhenius equation but with the temperature dependence of both terms, although such dependence is almost negligible when  $E_a \gg RT$ , which is the case for most chemical reactions.

The equation 2.21 suggests an inversely proportional dependence between  $E_a$  and  $k$ , that is, a low value for  $E_a$  is related with a high value for  $k$ , and therefore with a fast reaction, while a high value for  $E_a$  means a slow reaction with a low value for  $k$ . On the other hand, in that same equation (2.21), a directly proportional dependence between  $k$  and the temperature is observed. The rapid proportional increase of  $k$  with  $T$  can be mainly attributed to the increase in the number (or frequency) of collisions whose energy exceeds the critical value  $E_a$ . Related to this frequency of collisions, an underlying factor may be defined in terms of the space or volume in which the reaction is allowed to occur. Assuming that such consideration of the volume of the container ( $V_{container}$ ), as well as the density of the particles ( $\rho_{Particles}$ ), is contained in a factor denoted by  $z_{coll}$ , a good representation for such factor is expressed in the following relationship:

$$z_{coll} = \sigma_A \langle u \rangle_A \rho_A , \quad (2.22)$$

where  $\sigma_A$  is the cross-section collision,  $\sigma_A = \pi d^2$ , where  $d$  is the diameter of particles  $A$ . The terms  $\langle u \rangle_A$  and  $\rho_A$  correspond to mean speed and number density of particles  $A$ , respectively. The 2.22 can be re-written as:

$$z_{coll} = \pi d_A^2 \left( \frac{\Delta x}{\Delta t} \right) \rho_A \approx \frac{V_{container} \rho_{Particles}}{\Delta t} , \quad (2.23)$$

where  $\Delta t$  represents the time interval considered for the collision count.

According to the equation 2.22, the frequency of molecular collision density between identical particles,<sup>15</sup> for example, between particles  $A$ , can be represented by:

$$Z_{AA} = \frac{1}{2} \rho_A z_{coll} = \frac{1}{2} \rho_A^2 \sigma_A \langle u \rangle_{r,A} , \quad (2.24)$$

being  $\langle u \rangle_{r,A}$  the reduced mean speed of particles  $A$  defined by:

$$\langle u \rangle_{r,A} = \sqrt{\frac{8 k_B T}{\pi \mu_A}} = 2^{1/2} \sqrt{\frac{8 k_B T}{\pi m_A}}, \quad (2.25)$$

where  $\mu_a$  is the reduced mass of  $A$ ,  $\mu_A = m_A/2$ , where  $m_A$  is the mass of particles  $A$ . Therefore the equation 2.24 results in:

$$Z_{AA} = \frac{1}{2} \rho_A^2 d_a^2 \pi 2^{1/2} \sqrt{\frac{8 k_B T}{\pi m_A}} = 2 \rho_A^2 \sqrt{\frac{8 \pi k_B T}{m_a}}, \quad (2.26)$$

The terms  $k_B$  and  $T$  have the usual meaning of Boltzmann constant and the absolute temperature, respectively. For the case of the heterogeneous bi-molecular reactions, for example, between a particle  $A$  and a particle  $B$ , the frequency of molecular collision density could be adapted for as follows:

$$Z_{AB} = \rho_A \rho_B \sigma_{AB} \langle u \rangle_{r,AB} = \rho_A \rho_B d_{AB}^2 \sqrt{8 \pi \frac{k_B T}{\mu_{AB}}}, \quad (2.27)$$

in which the reduced mass  $\mu_{AB}$  of particles  $A$  and  $B$ , and the mean of its respective diameter, that is  $d_{AB} = (d_A + d_B)/2$ , are used.

Incorporating in the equation 2.21 the factor of collisions defined previously in the equation 2.33, for generality, the Arrhenius equation can be re-written as:

$$k = Z_{AB} \exp \frac{-E_a}{RT}. \quad (2.28)$$

However, the description given for the factor  $Z$  ignores the hindrance effect between molecules and the relative orientation, which plays a crucial role during a chemical reaction. It is known that for a reaction to occur, two molecules must collide in the correct orientation.<sup>15</sup> Even in the most controlled experiment, all the molecules involved in the reaction do not collide in a proper orientation; therefore, it is convenient to include a probability of collision factor defined by a term  $\mathcal{P}$ ,<sup>15</sup> for which the equation 2.28 results in:

$$k = \mathcal{P} Z_{AB} \exp \frac{-E_a}{RT}. \quad (2.29)$$

## 2.4 Transition State Theory

In the 1930s, Henry Eyring proposed a theoretical description of reaction rates known as the *Transition State Theory* (TST), also known as *Activated Complex Theory*. This theory provides a theoretical description of reaction rates without involving complicated quantum mechanical calculations.<sup>12</sup> This theory's conceptual idea suggests the formation of the species  $AB^*$ , called activated complex, that occurs at the transition state, an intermediate state during the chemical reaction before the product formation. The activated complex is characterized by being unstable species, with a lifetime of a few periods of molecular vibration in some reactions ( $10^{-14}$  s).

In order to support the theory, some significant assumptions are needed. The first one considers that equilibrium occurs between the reactants and the activated complex. Furthermore, it is assumed that the reaction coordinate describing decomposition of the activated complex can be mapped onto a single energetic degree of freedom of the activated complex.<sup>12</sup> Taking this in mind, the 2.30 and 2.31 equations represent the equilibrium between reactants, activated complex, and the decay of the activated complex to form the product respectively.



This mechanism proposed could be used to develop an expression for the product formation rate, based on the set of differential equations, by considering the assumption of equilibrium between reactants and the activated complex. After a multi-step mathematical development, the central equation of TST, that relates the rate constant of the chemical reaction to the molecular parameters for species involved in the reaction,<sup>12</sup> is reached, and which is expressed by:

$$k = \frac{k_B T}{h c^\circ} K_c^* , \quad (2.32)$$

Where  $c^\circ$  represents the standard concentration, set to 1 M,  $k_B$  corresponds to the Boltz-

man constant,  $T$  is the temperature of the system, and  $K_c^*$  is the equilibrium constant of the reaction 2.30, which is related to the partition functions of the activated complex and reactants that describes the measure of the volume occupied by the system in a phase space.

The common Eyring equation is obtained by relating the results obtained by activated complex theory and the well-known thermodynamic descriptions for the Gibbs energy variation, such as:

$$\Delta G^* = -RT \ln K_c^* . \quad (2.33)$$

In the equation 2.33,  $\Delta G^*$  represents the difference in Gibbs energy between the transition state and reactants and  $R$  is the gases universal constant. Taking an expression for  $K_c^*$  from 2.33, the expression for  $k$  becomes:

$$k = \frac{k_B T}{h c^\circ} \exp^{-\Delta G^*/RT} . \quad (2.34)$$

This equation contains the temperature dependence of the rate constant. Furthermore, using the definition for  $\Delta G$  in terms of enthalpy and entropy variations,  $\Delta G = \Delta H - T\Delta S$ , the Eyring equation, also known as Eyring-Polanyi equation, is finally obtained:

$$k = \frac{k_B T}{h c^\circ} \exp \frac{\Delta S^*}{R} \exp \frac{-\Delta H^*}{RT} . \quad (2.35)$$

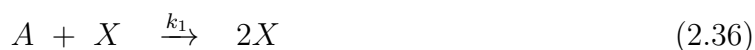
The equations from 2.32 to 2.35 were derived, taking into account the mechanism of reaction, frequency of collisions between molecules, as well as the energy asociated to them. The conjunction of these factors allows determining the reaction rate and its dependence on the experimental condition and parameters that optimize the reaction. Eyring's theory argues that both, chemical reactions and different physical processes, such as electron transfer, conductivity, viscous flows, molecular diffusion, are rate-controlled processes and require activated energy to move from the initial state to the final state.<sup>16</sup>

## 2.5 Oscillating Reactions

The standard models of chemical kinetics analyze systems in which the reactants are combined to obtain products until equilibrium, that is, in the absence of macroscopic

variation in reactant or product concentrations with time. However, in some reactions, the equilibrium never reached due to a periodic supply of reactants or products' removal. These particular reactions are referred to as oscillating reactions, with kinetic features as nonlinearity in the differential equations associated with them and the species' feedback. For a while, this kind of reaction was considered a strange phenomenon; however, they are found in a wide variety of systems in biology (cellular energy, chemotaxis) and chemistry (combustion, film growth).<sup>2</sup>

The first plausible mechanism related to the oscillating processes was proposed in 1920 by Lotka and then validated by Volterra a few years later to explain ecological oscillations,<sup>17</sup> through the following mechanism:



For whose dynamic equations were applied the law of mass action.<sup>10</sup> This mechanism has frequently been used to explain chemical processes undergoing periodic behavior.

Currently, the mechanism is given in 2.36 - 2.38 is known as the Lotka-Volterra mechanism and, frequently called as the predator-prey mechanism,<sup>12,18</sup> because this model describes the interaction between two animal populations, predator and prey, in time and space.<sup>18</sup> In such a mechanism,  $X$  is the prey,  $Y$  is the predator,  $A$  (reactant) is the birth/reproductive rate of a prey and  $B$  (product) is the dead of the predator. The initial increase in prey population promotes an increase in the predator population. Later, due to the predators consuming the prey, the prey population decreases and impresses a decrease in the predator population. Finally, this decline in predators allows the prey population to increase, and the cycle starts over again.<sup>12</sup>

Meanwhile, on the other hand, in 1921, Bray discovered a periodic reaction in a homogeneous solution through the decomposition reaction of aqueous  $\text{H}_2\text{O}_2$  in the presence of  $\text{IO}_3^-$  and  $\text{I}_2$ , involving autocatalytic reaction steps, that is, those in which a product speeds up the reaction. In this kind of reaction, repeated oscillations in the concentrations of one

or more species (intermediates or catalysts) are observed as a function of time. Notably, the reaction studied by Bray repeated oscillations in the  $I_2$  concentration were showed. The periodically repeated changes in concentration of some species in the reaction could imply a sequence of color, pressure, or temperature changes in the mixture of reactions, which is very attractive to be studied.

Due to the complexity of these reactions, it was not until the years 1950–1970, by experimental work of Belousov and Zhabotinskii and the theoretical work of Prigogine, among others, that it was firmly established the basis of oscillating reactions,<sup>17,19,20</sup> being considered as reactions out of equilibrium, which means that the chemical system must be far from its equilibrium condition during the chemical reaction for the periodic oscillations to occur.

Subsequently, differential rate expressions associated with this kind of reactions, whose mechanism is given by 2.36-2.38 equations, can be represented by the following equations:

$$\frac{d[X]}{dt} = 2k_1 [A][X] - k_2 [X][Y] \quad (2.39)$$

$$\frac{d[Y]}{dt} = 2k_2 [X][Y] - k_3 [Y] . \quad (2.40)$$

It is worth mentioning that, according to the proposed mechanism, the rate of this reaction is independent of the concentration of species  $B$  formed during the reaction. By graphing the 2.39 and 2.40 equations, the oscillating behavior of the concentrations of  $X$  and  $Y$  species is observed, as is shown in figure 2.2. For the case in which the concentration of  $A$  species is kept constant by supplying continuously an amount of  $A$  as the reaction proceeds, being the concentrations of intermediates species  $X$  and  $Y$  the most relevant in determining the reaction rate.

Calculating the concentrations of  $X$  and  $Y$ , through solving differential rate equations given in 2.39 and 2.40, requires to employ Euler method due to it provides the more straightforward way to predict how reactants and products concentration will vary for a kinetic scheme<sup>Engel2007</sup> by taking into account the initial concentration of  $A$  specie, denoted by  $[A]_0$ . Expressions for  $X$  and  $Y$  concentrations obtained from analysis demonstrate the

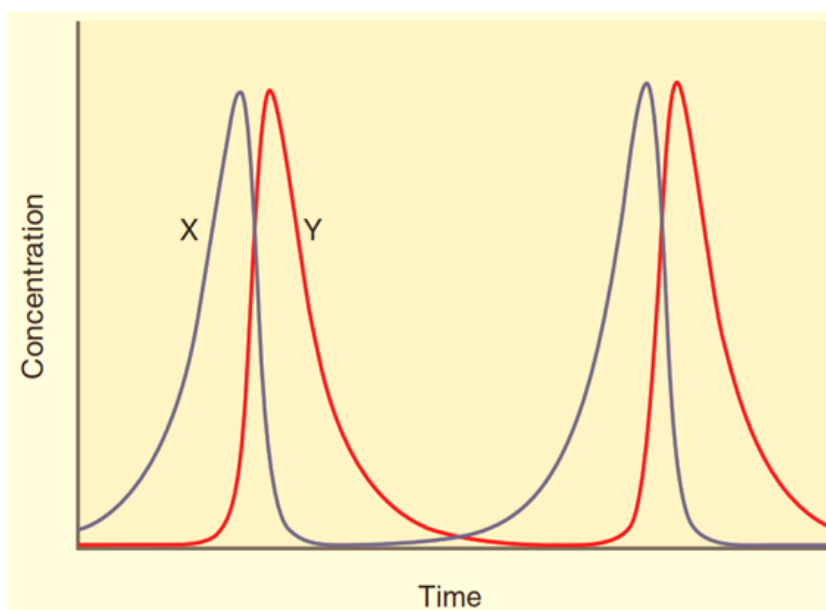


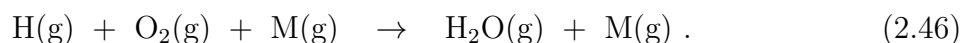
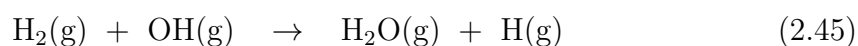
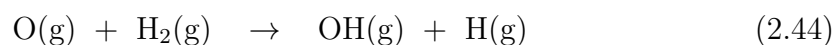
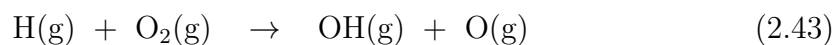
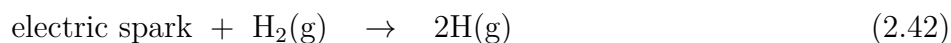
Figure 2.2: Oscillatory behavior of intermediate concentrations from the Lotka-Volterra mechanism [12].

oscillating behavior for both species' concentrations. Some defining features of this behavior can be obtained, such as the oscillation period and the time in which the maximum concentrations of species are reached.

The particular phenomena of feedback contemplated in oscillating reactions can be explained through the mechanism of the conversion from hydrogen and oxygen to water, represented by the equation:



A simplified mechanism for this reaction corresponds to:<sup>21</sup>



This mechanism involves some feedback steps; that is, one step's product in a reaction



sequence affects other reaction steps in the sequence. This effect is generally modeled with nonlinear differential rate expressions in the description of the mechanism to activate or inhibit these reactions.<sup>2,22</sup> The behavior of linear and non linear expressions can be described by the to the coefficient of reaction advancement, denoted by  $\xi$ , that is:

$$\xi = \frac{[\text{H}_2]_0 - [\text{H}_2]}{[\text{H}_2]_0} . \quad (2.47)$$

In the presence of an excess of  $\text{O}_2$ , the  $\text{H}_2$  follows a first-order reaction with a rate analytically represented by the linear differential equation given in the equation 2.48, and graphically represented by the purple curve in figure 2.3.

$$\frac{d\xi}{dt} = k(1 - \xi) . \quad (2.48)$$

In the case in which the oxygen is not in excess, the reaction rate should be analytically represented by the non-linear differential expression, given by 2.49, and graphically by the red curve in figure 2.3.

$$\frac{d\xi}{dt} = k(1 - \xi)^2 . \quad (2.49)$$

However, from the mechanism shown for the reaction of molecular hydrogen and oxygen, it is easy to perceive that the rate of the reaction cannot be represented as a simple second-order reaction due to feedback steps involved, that is, the rate of the reaction to increases as hydroxyl radical is formed, and then decreases as the reactants are consumed. This fact implies that the rate expression should be represented by:

$$\frac{d\xi}{dt} = k\xi(1 - \xi) , \quad (2.50)$$

with a graphical representation shown with the blue curve in figure 2.3.

The equation 2.50 is well related to the general relationship for quadratic auto-catalytic reaction, represented by the following equation:



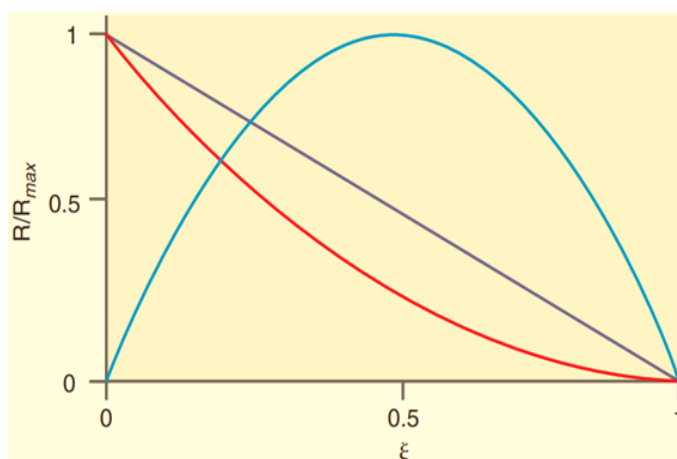


Figure 2.3: Illustration of the dependence of the reaction rate on the coefficient of reaction advancement  $\xi$ . Retrieved from [12].

with an expression rate given by:

$$rate = k[A][B] \quad (2.52)$$

The Lotka-Volterra mechanism has been commonly applied in the description of complex chemical reactions and biological processes. However, it has extended to a wide range of systems and processes, such as economic activity, wildlife, populations, and even the spread of the disease,<sup>18</sup> establishing an analogy between the "predator-prey" mechanism with the process of interest.

# Chapter 3

## Mathematical Models in Epidemiology

Mathematical modeling has been gaining great importance in epidemiology because it allows to describe and predict infectious disease dynamics at a population level from an individual-level knowledge of epidemiological factors. Furthermore, the long-term behavior from the early spread dynamics and the impact of vaccination on the spread of infection also can be modeled. The models' precision will depend on the quality of data available and the time frame in which the results are obtained.<sup>23-25</sup>

To formulate a good model for a particular problem, it must be sustained on three claims: accuracy, transparency, and flexibility.<sup>23</sup> Accuracy refers to the capacity to reproduce the observed data and reliably predict future dynamics. On the other hand, transparency refers to as the capacity to understand the correlation between model components and their influence on dynamics. Finally, flexibility is the ability of the model to be adapted to new emerging scenarios. A well representative model allows analyzing a given process, estimating its dynamics, and providing predictions about its behavior.

Due to the models' precision, some governments have been using them to analyze epidemics in order to develop different strategies and policies, allowing them to model different scenarios and estimate the possible results. For example, in 2001, in the United Kingdom (UK), predictive models were used in two different situations: one of them during the foot-and-mouth epidemic, and then another during the potential bioterrorist release

of smallpox.<sup>4</sup> For the case of the foot-and-mouth epidemic, the researchers proposed to respond to two questions, the first one: if the epidemic was controlled, and the second one: if any additional targeted culling would lead to a reduction in the total loss of livestock. Three models were used and configured to perform the analysis based on different known dynamical complexity judgments. Models presented their advantages and problems; they lead to a similar conclusion: the epidemic will be large scale, and locally targeted culling would reduce the overall loss of livestock by dramatically reducing the number of cases.<sup>4,26</sup>

Against the smallpox bioterrorist weapon scenario, the principal models used were those from Meltzer<sup>27</sup> and Halloran<sup>28</sup> rather than the aforementioned models, which showed high sensitivity to the implied variables and scenarios. However, due to the increase in computing efficiency, model sensitivity, and the quality of data retrieved, models give a good approximation to biological phenomena and, even more, describe an infection's dynamic profile in an epidemic breakout.

In general, the principal stochastic biological models consider that the progress of an infectious disease is defined qualitatively in terms of the pathogen's growth rate within the host and the interaction between the pathogen and the host immune response.<sup>23</sup> In figure 3.1 shows a simple representation of a dynamic profile of infection, where different stages of the pathogen inside the host's immune system go through are illustrated. During stages, and depending on the host's ability to transmit the pathogen, an individual can be classified within a particular category. Initially, no pathogen is present, but the host is *susceptible* to infection, and just a low-level nonspecific immunity is within the host. Once the host comes in contact with an infectious individual and becomes infected, it is time zero of infection is considered, and from this moment, the abundance of the parasite within the host grows over time. During this early phase, the individual may exhibit no apparent signs of infection, and the abundance of the pathogen may be too low to allow further transmission — individuals in this phase are said to be in the *exposed* category. Once the parasite level is sufficiently large within the host, the potential exists to transmit the infection to other susceptible individuals; the host is considered as an *infectious* individual. Finally, once the immune system of an individual has cleared the parasite and the host is therefore no longer infectious, they are referred to as *recovered*.<sup>23</sup>

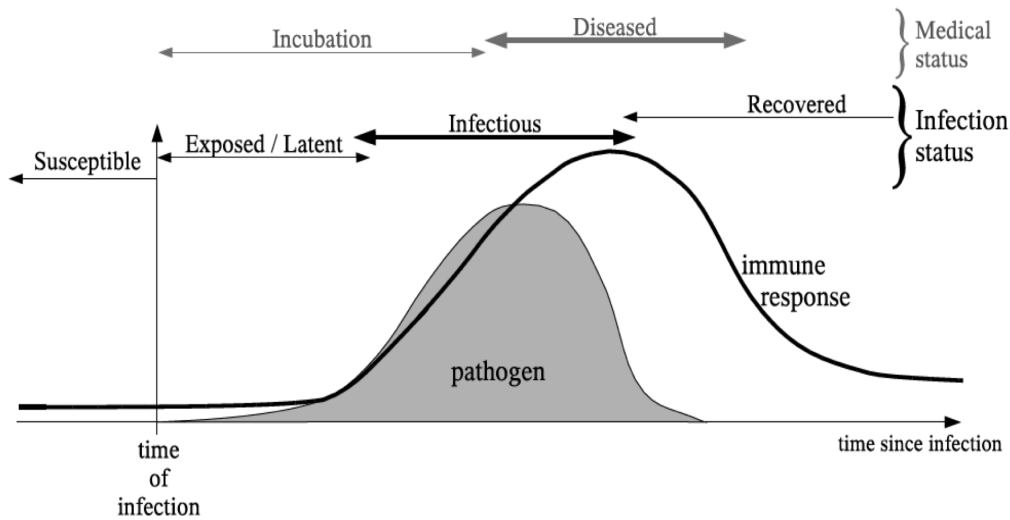


Figure 3.1: Representation of the time-line of infection, showing the dynamics of the pathogen (gray area) and the host immune response (black line) as well as labeling the various infection classes: susceptible, exposed, infectious, and recovered. Note that the diseased period, when symptoms are experienced, is not necessarily correlated with any particular infection class. Retrieved from [23].

The most common mathematical models to evaluate the transmission dynamics of infectious diseases are known as *Compartmental Models*, in which the population sample is distributed into labeled compartments.<sup>4</sup> Each labeled compartment represents a state of a population individual through time during an epidemic breakout. Once the population is distributed, the model can be performed in a deterministic manner (using differential equations) or stochastic (random framework) depending on the research's necessities. These models are based on the deterministic formulation of chemical kinetics, which allows the analysis of epidemics, the estimation of the diseases' properties, and the evaluation of strategies of its mitigation.<sup>29</sup> When establishing the analogy between disease transmission and chemical reactions, the pathogen transmission rate is represented by the temporal variation of the concentration of the species involved in the chemical reaction, considering that the transmission process occurs as a reaction sequential chemistry. The different species involved in the transmission process representing the population members are categorized according to their infection status, which shows some characteristics or attributes. The categorization before mentioned, the four types of individuals: susceptible, exposed, infected, and recovered, allows defining different compartmental epidemic models, depending

on the type of species considered in its description. For example, the *SIR model* involves susceptible, infected, and recovered species, and as can be seen, its name is an acronym with the initial letters of the category of individuals involved. On the other hand, the *SEIR model* also involve exposed individuals in its description. Other descriptive compartmental models exist, distinguishing each other according to the types of individuals considered, and the modifications (if applicable) applied to the proposed mechanism of transmission.

The aforementioned dynamic models capture the information about the behavior of the population against a pandemic breakout. These results allow the estimation of evolution over time of the infectious disease and the effect of the moderation (or relaxation) of the distancing/isolation measures, providing preventive measures and strategies to be implemented.

In this work, a set of compartmental model analogs: SIR, SEIR, and SEIRD, are proposed to establish predictions of an epidemic outbreak. These models are based on classic epidemiological models using chemical kinetic principles, and, as a consequence, they are not only based on stochastic approaches but also based on phenomenological approaches.<sup>30</sup>

### 3.1 The SIR dynamic model of infectious diseases

The compartmental SIR model is an epidemiological model for acute diseases in which the host is categorized into three compartments occupied by the Susceptible, Infected, and Recovered individuals. The kind of individuals occupying the susceptible compartment describes an individual that has not been exposed previously to the pathogen (disease). On the other hand, the infected compartment is occupied by every individual that currently has the pathogen, and finally, the recovered compartment consider every individual who no longer presents the infection after having suffered it.<sup>5</sup>

Figure 3.2 corresponds to a representative flowchart of the SIR model. The solid black arrows show the transitions of an individual between the Susceptible (S) and Infected (I) classes and the Infected (I) and Recovered (R) classes, representing the temporal direction of the model. The dotted gray arrow represents the fact that the infectious disease level

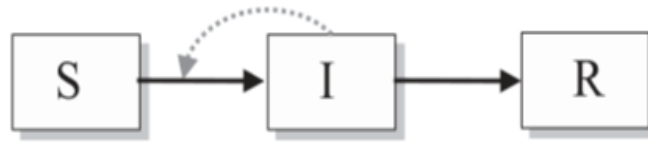
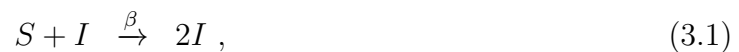


Figure 3.2: Schematic SIR flowchart. [23]

influences the rate at which a susceptible individual moves into the infected class. The SIR model dynamics are described by a set of differential equations whose parameters of transmission and recovery rates are included. These differential equations result in the assumptions taken into account in the model related to the research's necessities and the disease characteristics. Commonly, the SIR model considers a scenario where a few infectious agents are introduced into a closed population leading to a quick expansion of the disease. This phenomenon is considered an epidemic breakout, for which demographic processes (births, deaths, or migration) are not considered.<sup>4</sup> Furthermore, the transmission and recovery rates denoted as  $\beta$  and  $\gamma$ , respectively, are defined for homogeneous mixing, discarding the intricacies that affect the contact pattern.

The mechanism represented by the SIR model, in analogy to a chemical reaction mechanism, may be described as:



where  $\beta$  and  $\gamma$  parameters represent the transmission and recovery rates of the infectious disease, respectively. The set of differential equations to describe this mechanism, namely, the temporal variation of the population in each compartment considered in the SIR model,

corresponds to:

$$\frac{dS}{dt} = -\beta SI , \quad (3.3)$$

$$\frac{dI}{dt} = \beta SI - \gamma I , \quad (3.4)$$

$$\frac{dR}{dt} = \gamma I . \quad (3.5)$$

The equation 3.3 represents the temporal evolution of the susceptible class, taking into account the probability with which their changes occur, represented by  $\beta$ . This parameter is commonly referred to as the "force of infection",<sup>31</sup> denoted by  $\lambda$ , being a measure for the probability per capita of getting the infection.<sup>32</sup> The following equation 3.4 represents the temporal changes of infectious class, incorporating the  $\gamma$  parameter, representing the recovery rate. The inverse of this parameter,  $(\gamma)^{-1}$ , represents the average recovery time. Finally, the equation 3.5 represents the temporal evolution of recovered individuals class, taking into account the recovery rate  $\gamma$  of all infected individuals.

The set of equations 3.3-3.5 should be solved numerically, considering the initial conditions for the susceptible, infected and recovered population given by  $S(t = 0) = S_0 > 0$ ,  $I(t = 0) = I_0 > 0$ , and  $R(t = 0) = Rec_0 = 0$ . The values for  $S_0$ ,  $I_0$ , and  $Rec_0$  are assigned according to the region's data to evaluate, representing the total population, the number of infected individuals at the beginning of the analysis and the number of recovered individuals, respectively. Also, it is considered the additional condition that  $S + I + R = 1$ , due to this summation involves all species considered in the model. The solutions that result from this set of differential equations are plotted and shown in figure 3.3.

In figure 3.3 can be perceived the behavior of the resultant curves for functions  $S(t)$  (blue curve),  $I(t)$  (orange curve) and  $R(t)$  (green curve), after solving the respective differential equations.



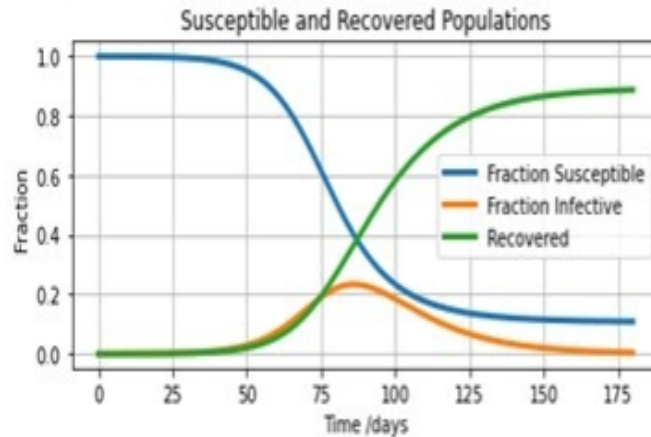


Figure 3.3: Sample SIR chart with an initial conditions of  $S(0) = 1000, I(0) = 1, R(0) = 2.5$  Population Fraction:  $1/1000$ . The variance trough time of S,I and R is observed.

## 3.2 Basic Reproductive Ratio ( $R_0$ ) - Threshold Phenomena

From the equation 3.4, it can be assumed that the evolution of the epidemic depends on the interplay of two parameters,  $\beta$  and  $\gamma$ , representing the transmission and recovery rates. It has been reported by Kermack and McKendrick,<sup>5</sup> and widely accepted, that if the initial fraction of susceptible individuals meet to condition  $S_0 < \gamma/\beta$ , then the infection tends to fall through, that is,  $dI/dt < 0$ . This result is referred to as the “threshold phenomenon.” It is assumed that is identified a quantity or proportion of the susceptible population depends on the epidemic’s characteristics, such that if the threshold value is exceeded, then the epidemic propagates. This threshold factor is precisely given by  $\gamma/\beta$ ,<sup>33</sup> which also is called relative removal rate, requiring to be small enough to allow a disease to spread.

One of the most important quantities in epidemiology is precisely the inverse of the relative removal rate, which is called *primary reproductive ratio* and denoted by ( $R_0$ ). This ratio is defined as the "average number of secondary cases arising from an average primary case in an entirely susceptible population".<sup>23</sup> Remarkably, the primary reproduction ratio estimates the maximum reproductive potential for infectious disease and allows to know the impact of the different implemented control policies on the virus spread varies through

time.<sup>34,35</sup> Considering the parameter  $R_0$ , the threshold phenomena can be re-expressed into a new concept, that is, the invasion of a pathogen into a susceptible population is defined by  $R_0 > 1$ . This concept correctly contextualizes because if the infection cannot successfully transmit onto more than one new host, then the infection will not spread.<sup>36</sup>

For an epidemic, the value of  $R_0$  will be given by considering the particular and specific aspects of the disease and the demographic characteristics of a human population. Among these characteristics, the contact structure, rural-urban gradients, and demographic rates are included. Different values for  $R_0$  can be obtained for the same disease affecting different regions due to the demographics characteristics of each population.<sup>23</sup> In the table shown in figure 3.4 are indicated some value of  $R_0$  for different infectious diseases affecting a different kind of population.

<i>Infectious Disease</i>	<i>Host</i>	<i>Estimated <math>R_0</math></i>	<i>Reference</i>
HIV	Domestic Cats	1.1–1.5	Smith (2001)
Rabies	Dogs (Kenya)	2.44	Kitala et al. (2002)
Phocine Distemper	Seals	2–3	Swinton et al. (1998)
Tuberculosis	Cattle	2.6	Goodchild and Clifton-Hadley (2001)
Influenza	Humans	3–4	Murray (1989)
Foot-and-Mouth Disease	Livestock farms (UK)	3.5–4.5	Ferguson et al. (2001b)
Smallpox	Humans	3.5–6	Gani and Leach (2001)
Rubella	Humans (UK)	6–7	Anderson and May (1991)
Chickenpox	Humans (UK)	10–12	Anderson and May (1991)
Measles	Humans (UK)	16–18	Anderson and May (1982)
Whooping Cough	Humans (UK)	16–18	Anderson and May (1982)

Figure 3.4: Estimated Basic Reproductive Ratios for different diseases. [23]

### 3.3 The SEIR model: Adding a latent period to SIR model

The SEIR model is a variant of the classic SIR model, and the modification consists of including a new class of individuals to consider those hosts that cannot be categorized as susceptible, infectious or recovered, due to very low abundance of the pathogen in the host, as to be considered an active agent for transmission to other hosts, at least for a

meanwhile.

Some specific pathogens (bacteria cells or virions) require a period to reproduce rapidly within the host. During this period, the load of these pathogens is not enough for the host to transmit the disease. In that case, it is necessary to introduce a new compartment for these individuals who are "infected" but not yet "infectious".<sup>23</sup> The compartment is referred to as *Exposed* (E), and following the idea for the further model, this new model includes the letter "E" in its name, that is SEIR model. In figure 3.5, by a flowchart, is schematized the process considered in the SEIR model. The mechanism representing the

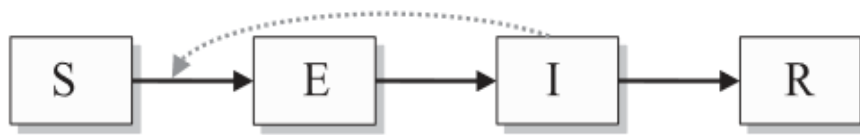


Figure 3.5: SEIR Flowchart.[23]

transitions considered in the SEIR model corresponds to:

$$S + I \xrightarrow{\beta} E, \quad (3.6)$$

$$E \xrightarrow{\sigma} I, \quad (3.7)$$

$$I \xrightarrow{\gamma} R, \quad (3.8)$$

The evolution rates of populations of different individuals considered in the model SEIR are described by the respective set of differential equations given below. In developing the SEIR equations had been considered the average duration of the latent period of the

infectious disease by  $\frac{1}{\sigma}$ .

$$\frac{dS}{dt} = \mu - (\beta I + \mu)S , \quad (3.9)$$

$$\frac{dE}{dt} = \beta SI - (\mu + \sigma)E , \quad (3.10)$$

$$\frac{dI}{dt} = \sigma E - (\mu + \gamma)I , \quad (3.11)$$

$$\frac{dR}{dt} = \gamma I - \mu R . \quad (3.12)$$

In these equations, the factor  $\mu$  represents the birth/death rate of a population. Noticing that, the SIR and SEIR models are qualitatively similar, particularly at equilibrium.<sup>23</sup> Indeed, both models behave similarly as long as the primary reproductive ratio  $\beta/\gamma$  and average infected period  $\frac{1}{\sigma}$  are identical. Regardless, the behavior difference between these models settles in the initial invasion stage due to the addition of exposed compartment (E) in the SEIR model. This stage slows down the dynamics producing a slower growth rate after pathogen invasion occurs due to the requirement for individuals to pass through the exposed class before contributing to the transmission of the disease.

### 3.4 SEIRD model: Modelling post death transmission

The SEIRD model, represented in the flowchart shown in the 3.6, is a variation of the classical SEIR model, in which transmission between infected and susceptible individuals occurs at an average rate  $\beta_I$  throughout infectiousness  $T_I$ , as is indicated in figure 3.6. This model also considers that, from individuals occupying the infected compartment, a fraction  $f$  of these individuals will die, while a fraction  $1 - f$  who will recover, assuming the gain of permanent host immunity against infection. Dead individuals are categorized in a new compartment denoted by D (*dead individuals*), including this letter in the name

of the model. Furthermore, this model includes an additional transmission route by which dead individuals can transmit to susceptible individuals at a special rate  $\beta_D$  throughout infectiousness  $T_D$ .<sup>37</sup>

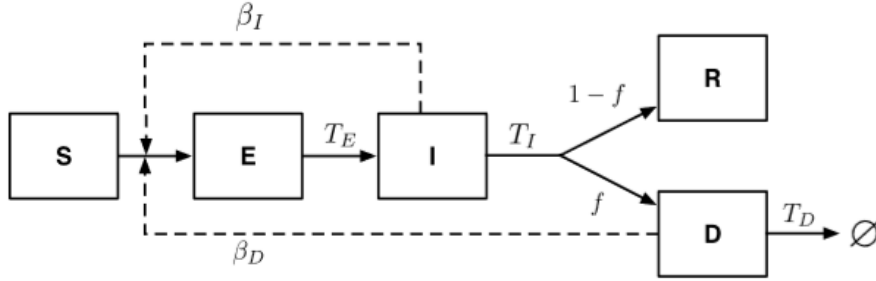


Figure 3.6: Schematic SEIRD Flowchart [37].

In the previous diagram, the solid arrows denote transitions between compartments, while the dashed arrows denote the transmission dependent of the interactions between  $S$  and  $I$  or between  $S$  and  $D$  (dead but still infectious). The different transmission rates are denoted by  $\beta_I$  and  $\beta_D$  and the average period of infectiousness are given by  $T_I$  and  $T_D$ , from one infected individual or one dead individual, respectively, while  $T_E$  refers to the latent period of the infection. Finally, the factor  $f$  is the fraction of individuals who die under the disease infection. For this model, the basic reproductive number ( $R_0$ ) is given by:<sup>37</sup>

$$R_0 = \beta_I T_I + f \beta_D T_D \quad (3.13)$$

The dynamics of the SEIRD model are similar to the SEIR model; it differs only in the R compartment, which stands for recovered individuals, and the D compartment for deceased individuals.<sup>37</sup> The mechanism associated with this model can be represented by:

$$S + I \xrightarrow{\beta_I} E, \quad (3.14)$$

$$E \xrightarrow{1/T_E} I, \quad (3.15)$$

$$I \xrightarrow{1/T_I} R, \quad (3.16)$$

$$I \xrightarrow{1/T_I} D, \quad (3.17)$$

$$D + S \xrightarrow{1/T_D} E. \quad (3.18)$$

Based on this mechanism, the respective set of differential equations representing the evolution rates of the populations of different individuals considered in the SEIRD model corresponds to:

$$\frac{dS}{dt} = -\beta_I \frac{SI}{N} - \beta_D \frac{SD}{N}, \tag{3.19}$$

$$\frac{dE}{dt} = -\beta_I \frac{SI}{N} + \beta_D \frac{SD}{N} - \frac{E}{T_E}, \tag{3.20}$$

$$\frac{dI}{dt} = \frac{E}{T_E} - \frac{I}{T_I}, \tag{3.21}$$

$$\frac{dR}{dt} = (1 - f) \frac{I}{T_I}, \tag{3.22}$$

$$\frac{dD}{dt} = f \frac{I}{T_I} - \frac{D}{T_D}. \tag{3.23}$$

For the case in where the infection transmission by death hosts is controlled, and there is the presence of asymptomatic individuals, the SEIRD contagion dynamics can be adjusted as follows:

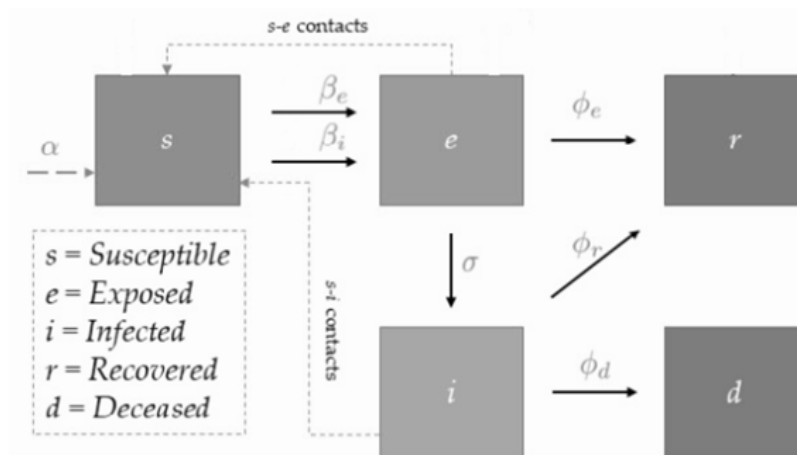


Figure 3.7: SEIRD variation with asymptomatic individuals Flowchart [38].

Sometimes, for simplicity, perhaps, this model does not consider natural deaths and new births. In that case, the set of differential equations representing the model can be

reinterpreted as follows:

$$\frac{dS}{dt} = -\beta_I SI - \beta_E SE , \quad (3.24)$$

$$\frac{dE}{dt} = \beta_I SI + \beta_E SE - \sigma E - \phi_e E , \quad (3.25)$$

$$\frac{dI}{dt} = \sigma_e - \phi_d I - \phi_r I , \quad (3.26)$$

$$\frac{dR}{dt} = \phi_r I + \phi_e E , \quad (3.27)$$

$$\frac{dD}{dt} = \phi_d I . \quad (3.28)$$

Here, the variable  $\sigma$  is the inverse of the incubation period,  $\phi_e$  is the asymptomatic recovery rate,  $\phi_r$  is the infected recovery rate,  $\phi_d$  is the infected mortality rate,  $\beta_e$  is the asymptomatic contact rate,  $\beta_I$  is the symptomatic contact rate.<sup>18</sup>

# Chapter 4

## Novel Zoonotic Epidemic: COVID-19

### 4.1 Historical worldwide Zoonotics Epidemics

Throughout human history, pandemics with zoonotic origins constitute a critical threat to the human race. The black death (1348-1350), caused by the bacterium *Yersinia pestis* and spread by infected flea (*Xenopsylla cheopis*), and the Spanish Flu (1918-1919) caused by the H1N1 influenza A virus, are two of the most critical pandemics episodes. Perhaps the black plague does not have an official amount of produced deaths; the estimations establish that the plague affects between a third and one half of the total European population.<sup>39</sup> By its part, the lethality of the Spanish Flu left approximately 260,000<sup>40</sup> deaths only in Spain. Nowadays, and with the increasing expansion of human activities such as the domestication of exotic animals, hunting, animal husbandry practices, wet markets, and destruction of ecosystems, humans have been forcing human-animal interactions. These interactions confirm an essential basis for increasing the probability of cross-species pathogen transmission; furthermore, their combination with specific factors such as socioeconomic and demography is directly related to the increase in the probability of epidemic outbreak.<sup>41</sup> For example, at the beginning of the 20th century, the hunting and butcher of wild non-human primates in Africa led to the cross-infection (zoonotic transmission) of the simian immunodeficiency virus responsible for HIV pandemic.<sup>42</sup> Besides, in 2003, Yi Guan and colleagues<sup>43</sup> contribute to necessary research that supports the potential zoonotic origins of the SARS pandemic. They isolated the severe acute respiratory syndrome (SARS) CoV



from Himalayan palm civets (*Paguma larvata*), found traces of the virus in raccoon dogs (*Nyctereutes procyonoides*) and workers from the market. Furthermore, with the evidence achieved, they found a relationship between how the poor health conditions of a living-animal market (wet market) could facilitate the transmission between animal-human or even animal-animal of an infectious pathogen.

## 4.2 SARS-CoV-2: Pathogenesis and Characteristics

On March 13, 2020, OMS declared a new pandemic occasioned by a new coronavirus denominated as SARS-CoV-2 or COVID-19. The virus presents similarities in zoonotic origin and ineffectiveness to severe acute respiratory syndrome (SARS)-CoV and the Middle East respiratory syndrome (MERS)-CoV. Also, it is responsible for producing coronavirus disease, which has been reported, as a potentially fatal disease with a remarkable capacity to transmit from person to person via direct contact or aerosols, which are commonly spread by coughing or sneezing from an infected individual. Structurally, SARS-CoV-2 has a glycoprotein that promotes the entry into cells using the ACE2 human receptor.<sup>44</sup> Indeed, the virus harbors a furin cleavage site between the boundary of  $S_1$  and  $S_2$  sub-units as shown in figure 4.1. On the one hand, the  $S_1$  sub-unit contains a receptor binding-domain that admit the host receptor angiotensin-converting enzyme 2, while on the other hand, the  $S_2$  sub-unit forms the six-helical bundle via the two-heptad repeat domain<sup>45</sup>

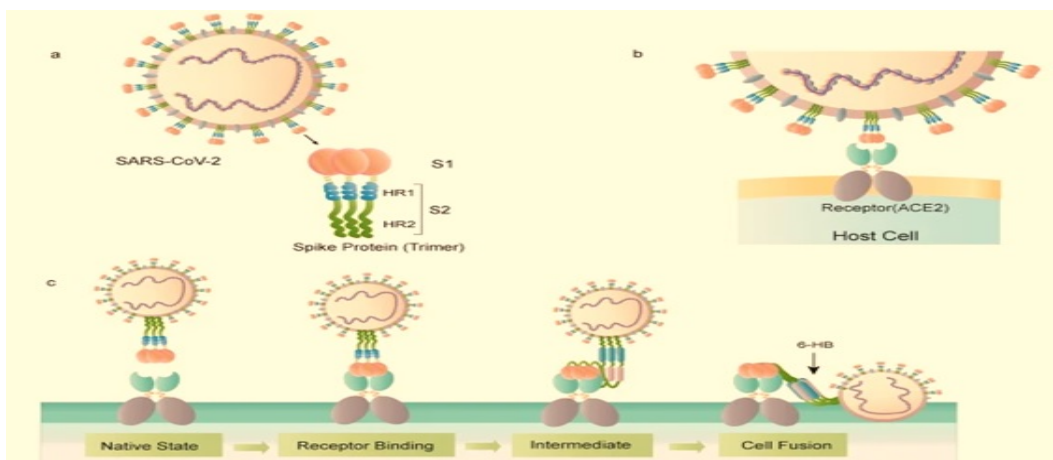


Figure 4.1: a) Schematic structure of the S protein of SARS-CoV-2. b) Protein-receptor (ACE2) interaction and c) Cell fusion process Retrieved from [45]

Once inside the cell, the virus can cause acute infections by evoking the host's antiviral immune responses. In most cases, the host's immune system tends to protect it against the infection killing the viral pathogen and stopping replication. However, sometimes, if the immune system does not control the infection initially, the virus will start to focus on ACE2 protein present in various human organs.<sup>46</sup> Furthermore, the ACE2 protein is present in abundance on lung alveolar epithelial cells and enterocytes of the small intestine.<sup>47</sup>

Once the infection reaches these organs, it induces an upregulation of the immune system to produce inflammatory cytokines. These cells can turn into immune cells and attack the inflammation occasioned by virus infection.<sup>48</sup> However, it also leaves a stew fluid of dead cells (pus)<sup>46</sup> and the immune dysregulation provokes a particular healthy issue defined as "cytokine storm" or hypercytokinemia, which is potentially fatal and a significant underlying factor in increased mortality of infected patients.<sup>49</sup> Furthermore, this is the underlying pathology of severe pneumonia (Observed in 4.2) and acute respiratory distress syndrome (ARDS),<sup>50</sup> two of the expected severe complications in Covid-19 disease.<sup>51</sup>

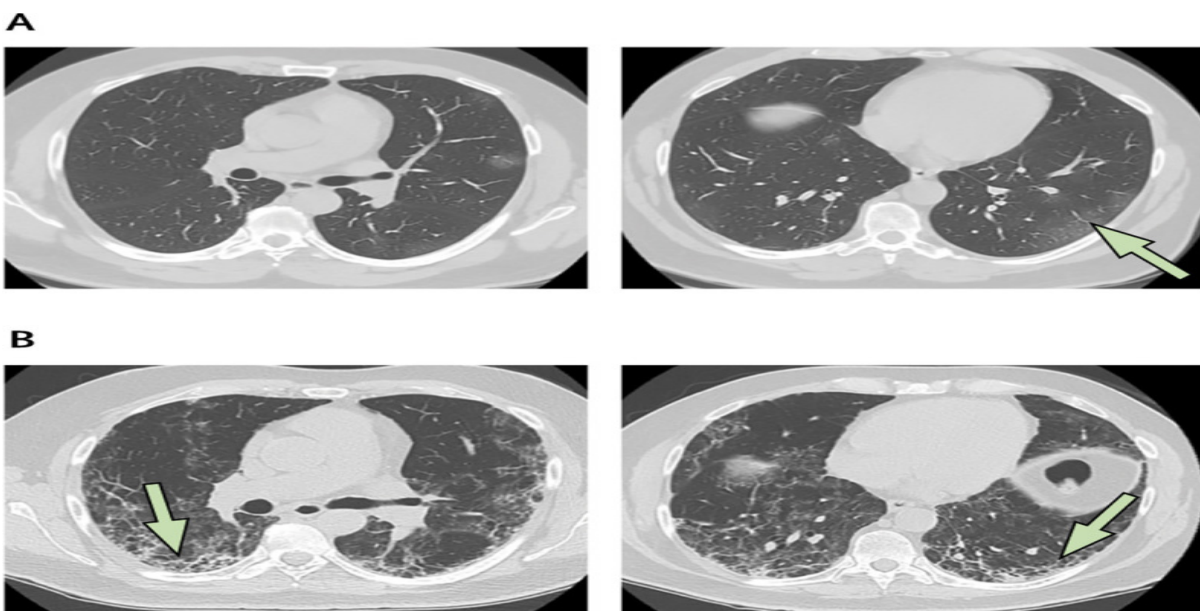


Figure 4.2: Lung CT of a patient with COVID-19. (A) Peripheral mild ground glass opacity's in the left lower lobe (arrow). (B) Three weeks later, at the same lung zones, the disease has rapidly progressed and fibrotic changes are now evident (arrows). Retrieved from [52]

However, since Coronavirus disease 2019 (COVID-19) is an emerging infectious disease, risk factors for the clinical outcomes of COVID-19 have not yet been well delineated,

requiring more research to establish them.<sup>51</sup>

### 4.3 COVID-19 Pandemic

COVID-19 dramatically worsened over a short time, provoking extreme societal, economic, and political disruption worldwide.<sup>53</sup> For this situation, it received considerable global concern by governments and researchers in order to establish strategies against the fast spread of the virus. According to WHO<sup>54</sup> on November 2020, the virus has already infected around 38,394,169 globally, producing a total of 1,089,047 deaths to date.

In Ecuador, the first case of COVID-19 was reported on February 29, 2020, an imported case from Spain. Since then, 150,360 citizens were tested as COVID-19 positive and 12,306 reported as deaths by the illness in all the territory to November 17.<sup>6</sup> Anyway, due to the socio-economical characteristics of the population and the deficiencies of an healthcare system, Ecuador easily becomes one of the countries more affected by the pandemic with more than 1,000 excess deaths per million inhabitants and the highest excess percentage-excess deaths as a share of normal deaths for the same period.<sup>55,56</sup>

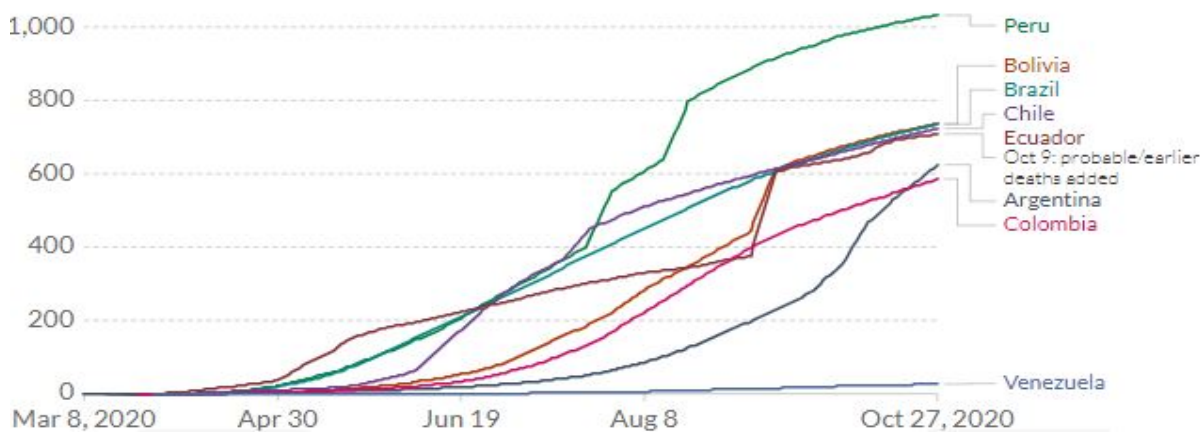


Figure 4.3: Cumulative confirmed COVID-19 deaths per million people. Coronavirus Pandemic (COVID-19)". Retrieved from: '<https://ourworldindata.org/coronavirus>'[57]

This situation could be evidenced by dramatic images recorded from Guayaquil City at the beginning of the pandemic (April - May 2020). Here, the healthcare system was overwhelmed by positive cases during the first weeks of the epidemic, provoking many deaths that even saturate the funerary services. Indeed, the city ran out of coffins leaving hundreds of corpses unburied and sometimes lying on the streets.<sup>58</sup>

However, it is a novelty virus; the approved vaccines for preventing infection are not accessible in necessary doses for all countries.<sup>59</sup> Also, there are no pharmaceutical options for an efficient treatment against COVID-19 disease. The available options are under continuous experimentation, and in some cases, the results do not differ much between treatment and placebo, putting its efficacy in controversy.<sup>60-62</sup> This situation complicates, even more, the Ecuadorian panorama making necessary to focus on strict Non-pharmaceutical interventions (NPIs) such as the constant use of face mask, social distancing policies, school closures, restrictions of gatherings, stay-at-home orders, non-essential business closure and scheduled curfew.<sup>6</sup> Perhaps the "simplicity" of these policies generates a positive effort in mitigating the spread of the virus<sup>63</sup>). Consequently, the Ecuadorian government could improve these NPIs to increase their effectiveness and mitigate the spread of the disease until pharmaceuticals interventions.

# Chapter 5

## Problem Statement and Objectives

### 5.1 Problem Statement

With 1093 deaths per million inhabitants, due to the coronavirus disease 2019 (COVID-19), as of April 6, 2020, Ecuador had one of the highest death rates from COVID-19 in Latin America. With a low health care capacity to handle pandemic outbreaks, the Ecuadorian government has a critical need for analytical tools to contain the spread of the virus in its territory, which is why it has focused on closing gaps in medical resources by establishing policies to decrease the spread, increase the availability of medical personnel, and improve the health system. Regardless, the pandemic is still not controlled across the country, with a high incidence of positive cases and deaths recorded per day.

Using stochastic models to evaluate the dynamics of epidemics, such as the SIR and SEIR models, the evaluation and analysis of the epidemiological behavior of the disease in Ecuador can be developed, obtaining information from the descriptive parameters of the dynamics of the epidemic. These models present the particularity that they are based on classical concepts of chemical kinetics, allowing the evolution over time of the population of infected individuals and the individuals susceptible to being infected. The implementation of this type of model under these assumptions offers a link, together with the fields of chemical kinetic-epidemic modeling, allowing the exchange of knowledge between sciences and generating new perspectives for analysis.

## 5.2 Objectives

### 5.2.1 General Objective

Implementation of descriptive mathematical models of epidemics based on the foundations of chemical kinetics as a tool for evaluating the dynamics of COVID-19 spread in Ecuador.

### 5.2.2 Specific Objective

- Search the data related to the reports of cases of infection by COVID-19, and compare them between the different official sources of information consulted, for a later appropriate selection.
- Adapt the information collected to the proposed strategies that allow a more optimal evaluation of the dynamics of the epidemic.
- Determine epidemiological indicators, such as transmission and recovery rates ( $\beta$  and  $\gamma$ ), and basic reproductive ratio ( $R_0$ ), based on the data collected from infected cases per day, during the period from March 13 - November 17, 2020.
- Propose a description of the dynamics of the epidemic and an analysis of the efficiency of the different restrictive policies, such as quarantine measures, curfew, implemented to contain the mitigation of the spread of the disease.

# Chapter 6

## Methodology

### 6.1 The SIR and SEIR Analogy

In chemical engineering, reactors are modeled with reactions and balances. The reactions identify chemical transformations of molecules through kinetic mechanisms, while mass and energy balances identify the nature and morphology of the reactor where transformations take place,<sup>64–66</sup>.

Classical compartmental models as SEIR and SIR distributes each member of a population, during an epidemic outbreak, into different compartments denoted as S for susceptible, (I) for infectious, (R) for recovered, and (E) for exposed in SEIR model.<sup>5</sup> Assuming that each person corresponds to a molecule of a specific chemical species, a chemical approach to SEIR and SIR model could be proposed.<sup>1</sup> For example, by considering the susceptible population as the reactant (S), Infectious or active infected people (I) as a reaction intermediate, and Recovered (R) as a product, a kinetic model representing the outbreak is given by equations 3.1 and 3.2. These equations describe the process by which susceptible individuals (S) can contract the disease if they come into contact with an infectious individual (I). The mechanism is analogous to an irreversible auto-catalytic chemical reaction 2.50 between a reactant species, in that case, represented by S, and catalyst species, represented by I. This situation occurs when it is assumed that zero delays exist between infection and the ability to transmit the disease between susceptible and infected individuals. Also, each reaction step is governed by the interplay of kinetic parameters

proposed by the Arrhenius equation.<sup>1</sup>

It is assumed that the kinetic mechanism associated with the disease spread takes place in a hypothetical batch reactor. Such a reactor is characterized by considering an inlet and outlet flow as nulls. Both conditions can be related to the restrictions in human mobility during the global lockdown imposed for governmental agencies, and in consequence, the batch reactor balances can reasonably predict the infection behavior.<sup>30</sup> Also, it is feasible to consider the susceptible population as the parameter that determines the active volume of the reactor. For COVID-19 disease, the recovered people are supposed to be immunized, and the reinfection parameter is not considered.<sup>67,68</sup>

For SEIR model, it is necessary to adapt the mechanism due to the presence of the *exposed individuals*, denoted by E compartment, and in consequence, the general mechanism is represented by equations 3.6 - 3.8. In that mechanism, the exposed compartment (E) and infectious compartment (I) are considered as intermediates of the reaction.<sup>1</sup> The SEIR model is a common variation of the SIR model in where, a latent period (E) is added.<sup>23</sup> Due to similarities between SIR and SEIR model, the chemical analogies would be similar in concept. Indeed, both mechanisms have the similar dynamics of a quadratic auto-catalytic reaction 2.50.

### 6.1.1 Models description

A stochastic system has been developed based on an already proposed batch-type numerical simulation.<sup>69</sup> The model dynamically characterizes the evolution of each species involved in the kinetic scheme. Kinetic constants for the reactions are described according to a modified Arrhenius-type law where the temperature-dependence is considered negligible due to the isothermal characteristics of the infection outbreak. By considering this, the virus spreading is then modeled, providing a phenomenological interpretation that monitors and predicts the time evolution of the SARS-Cov-2 spreading process.

For the proposed model, some assumptions were made. First, it is assumed that the spatial mix of the chemical species is uniform, and as a consequence, it will follow the law of mass action to model the rate at which susceptible and infectious individuals interact via bi-molecular, auto-catalytic reaction 2.50. For this model demographic variables are



considered as negligible. The number of new infections per unit time (incidence number) is considered as a symmetric, b- linear function of (S) and (I) and is defined as  $\beta(S)(I)$ . The second-order transmission rate constant  $\beta > 0$  follows the theory of collisions described in previous chapter 2.27 in consequence, is defined as the product of the average frequency of contacts of an individual and the specific transmission capacity of the disease  $R_0$ . Recovery transition is defined by the rate at which infectious individuals recover and is interpreted as a "deactivation" with the kinetics of first order. Also, its inverse  $\gamma > 0$  is the average time that an infected individual is infectious. From previous assumptions, sets of ODE resulting for each model, given before, are shown again for the convenience of analysis.

For SIR:

$$\frac{dS}{dt} = -\beta SI , \quad (6.1)$$

$$\frac{dI}{dt} = \beta SI - \gamma I , \quad (6.2)$$

$$\frac{dR}{dt} = \gamma I . \quad (6.3)$$

For SEIR:

$$\frac{dS}{dt} = \alpha S , \quad (6.4)$$

$$\frac{dE}{dt} = \alpha SI - \beta E , \quad (6.5)$$

$$\frac{dI}{dt} = \beta E - \gamma I , \quad (6.6)$$

$$\frac{dR}{dt} = \gamma I - \sigma R . \quad (6.7)$$

The set of ODE for SEIR model can be identified as two additional parameters, are,  $\alpha$  and  $\sigma$ . The parameter  $\alpha$  represents the transition rate of a susceptible individual to an

exposed individual, while the parameter  $\sigma$  is the transition rate from an infected individual to a recovered individual.

Each one of the previous ODE for both models requires the definition of initial conditions. These conditions are related to the numbers of initial active infected individuals  $I_0$ , initially recovered individuals  $R_0$ , and susceptible individuals  $S_0$ . Some conditions are considered trivial since they will be zero at the beginning of the epidemic, such as  $I_0$  and  $R_0$ . On the other hand,  $S_0$  is known since its value is obtained from the total individuals of a country population. The stability of this particular set of ODE has been primarily analyzed.<sup>70</sup>

As previously mentioned, the basic reproductive number  $R_0$  is obtained by the following relation:

$$R_0 = \frac{\beta}{\gamma} . \quad (6.8)$$

It is important to remark that  $R_0$  is constant in time, dimensionless, and represents a specific property of the disease and the population.<sup>23</sup> Under the analogy with chemical kinetics, since the catalyst's activity and longevity are embedded in  $\beta$  and  $\gamma$ , being  $R_0$  large if the catalyst has a high activity and remains active for a long time and vice versa.<sup>1</sup> Furthermore, the function of  $R_0$  factor can be explained by a chemical reaction analogy. If  $R_0 > 1$ , the injected catalyst particles deactivate faster than they catalyze to convert the reactant, S, into more catalyst, I, to propagate auto-catalytic.

### 6.1.2 Estimation of Transmission ( $\beta$ ) and recovery rate ( $\gamma$ )

The  $\beta$  and  $\gamma$  parameters corresponding to a specific population could be retrieved from the previous SIR ODEs by establishing some assumptions as follows:

$$\frac{dI}{dt} = \beta SI - \gamma I . \quad (6.9)$$

. At the beginning of the epidemic breakout there is no infection, that is  $I + R = 0$ , and the number of susceptible individuals is equivalent to the total population.<sup>71</sup> In consequence:

$$\frac{dI}{dt} \sim I(\beta - \gamma) \quad (6.10)$$

By integrating equation 6.10 the following expression is obtained:

$$I = I_0 \exp^{(\beta - \gamma)t} . \quad (6.11)$$

Then, by considering  $\beta - \gamma$  as a constant term ( $m$ ), the following equation could be proposed:

$$I \sim I_0 \exp^{mt} \quad (6.12)$$

.

Taking the logarithm of both sides, the equation 6.12 could be redefined as a common lineal equation with the form:

$$\ln I = mt + \ln I_0 = (\beta + \gamma)t + \ln I_0 , \quad (6.13)$$

where the slope  $m$  corresponds to a relation between the transmission and recovery rates, while the intercept between  $\ln I$  and time ( $t$ ), corresponds to a value related to the initial value for infected individuals in the period analyzed.

Then, the  $m$  value can be estimated from the log-plot data. On the other hand,  $\gamma$  value could be obtained from integrating the equation 6.3 giving the following expression:

$$R(t) = \gamma t I_0 . \quad (6.14)$$

Considering  $T$  as the recovery period, can be assumed that for  $t = T$  days the amount of recovered individuals takes the value  $R(T) = I_0$  when  $\gamma T = 1$ . In that case:

$$\gamma \approx \frac{1}{T} , \quad (6.15)$$

that is, the parameter  $\gamma$  corresponds to the inverse of recovery period. For a interval of time  $dt = a$ , the following expression can be proposed:

$$\frac{R(t+a)}{a} = \gamma I, \quad (6.16)$$

and therefore, the transmission rate ( $\gamma$ ) can be obtained by:

$$\gamma = \frac{R(t+1) - R(t)}{I(t)}. \quad (6.17)$$

From reported data obtained for number of infected and dead by COVID-19 individuals, the equation 6.17 is used for the determination of parameter  $\gamma$ .

# Chapter 7

## Results

### 7.1 Data Selection

The official epidemiological data of COVID-19 spread is published nearly every day by *Comité Nacional de Operaciones de Emergencia (COE)*, however, some inaccuracies are perceived during the recording period, which not only affects the reliability of the data but also generates problems in the statistical management of the data. These inaccuracies were perceived during specific dates, more precisely on the days: 6, 8, and 11 May 2020.<sup>6</sup> On these dates, around 2,461, 1,480, and 50 cases, respectively, were removed from analyzed data due to inconsistencies.

Therefore, a precise approach to the dynamics of COVID-19 in Ecuador requires the review and comparison of several databases to verify the information and appropriately select the data to be used. This stage of analysis is crucial to ensure that proposed models are suitably parameterized. The data selected from these sources were ordered and divided into different temporal sections, representing stages with different data management, social controls, implementing strategic policies by government entities, and the elimination of data corresponding to days with very high inaccuracies.

In the following table (table 7.1) are indicated the different temporal sections, taking into account the different lockdown periods imposed in Ecuador during the COVID-19 epidemic. For example, the first lockdown period, which began March 13<sup>th</sup>, was partitioned into three temporal sections, each denoted by LD-0-1, LD-0-2, and LD-0-3, respectively.

Partition of these periods depends on the behavior of the known data of infected population during these periods, and particularly in this first lockdown implemented, some imprecision in the management of data was perceived. The second stage considered for this analysis is denoted by the code CP-1, referring to the critical point related to how the first change in methodology by the government was implemented. The last LD-2 and LD-3 stages are considered due to policy relaxation in these periods, involving easing of restriction measures.

Table 7.1: Temporal sections for different periods during COVID-19 epidemic based in the social management in Ecuador.

Temporal sections.		
Code	Period of time	Information of period
LD-0-1	March 13 <sup>th</sup> - March 23 <sup>th</sup>	Lockdown period (1)
LD-0-2	March 24 <sup>th</sup> - April 11 <sup>th</sup>	Lockdown period (2)
LD-0-3	April 12 <sup>th</sup> - April 26 <sup>th</sup>	Lockdown period (3)
CP-1	April 27 <sup>th</sup> - June 1 <sup>st</sup>	Critical Point
LD-2	June 6 <sup>th</sup> - September 13 <sup>th</sup>	Partial Lockdown period
LD-3	September 14 <sup>th</sup> - November 11 <sup>th</sup>	Low restrictions

The methodology of the partitioning of the total period allows obtaining a more precise evaluation of data to estimate parameters associated with the transmission rate, that is, the  $\beta$  factor, which is necessary to perform the proposed SIR and SEIR analyses.

## 7.2 Epidemiological Characteristics of Ecuador

### 7.2.1 Confirmed Cases and their incidence

Retrieved data regarding the number of infected cases in Ecuador reported per day is shown in figure 7.1. These data were retrieved from database Ecuacovid research group,<sup>72</sup> Registro Civil<sup>73</sup> and COE Nacional,<sup>6</sup> the official bureau in charge of handling information regarding the COVID pandemic in Ecuador. The resultant figure shows an increasing daily

number of reported positive cases, with a mean value of 254 during the first stage of the epidemic breakout. The incidence number of positive cases per 100.000 inhabitants related to this value shows an estimation during the first period (February 28<sup>th</sup> to April 26<sup>th</sup>) with a value of 1.49. After April 26<sup>th</sup>, the mean value for daily reported cases increases rapidly to 1,751, with an incidence of 10.30. Then, a stabilization of the data occurs around May 11<sup>th</sup>, and since then, the mean value of positive reported cases per day is stabilized at 841, with an incidence number of 4.95.

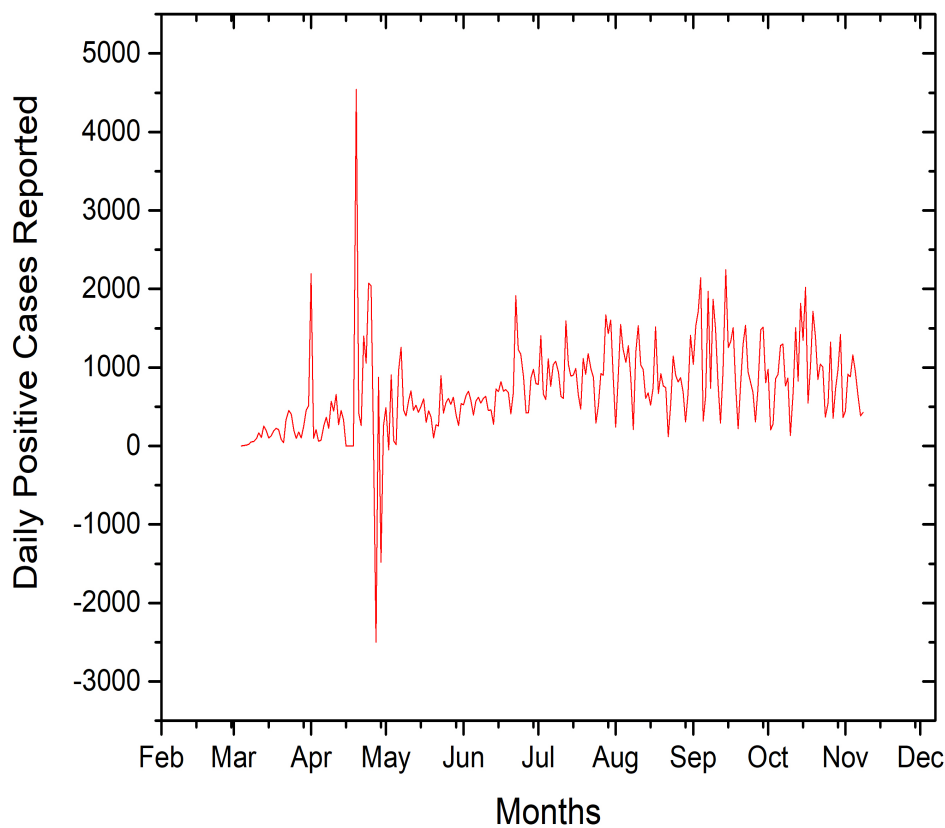


Figure 7.1: Daily variance of COVID-19 positive cases in Ecuador. Data Retrieved from online database: [6, 72, 73]

The cumulative for the positive reported cases is shown in figure 7.2, and as can be observed, on November 17<sup>th</sup> the curve still shows an upward trend with a total of 190,060 confirmed cases, with an incidence of 2.52. The sustained increase in the incidence factor is

related directly to the relaxation on curfew policies by government and the social fatigue.

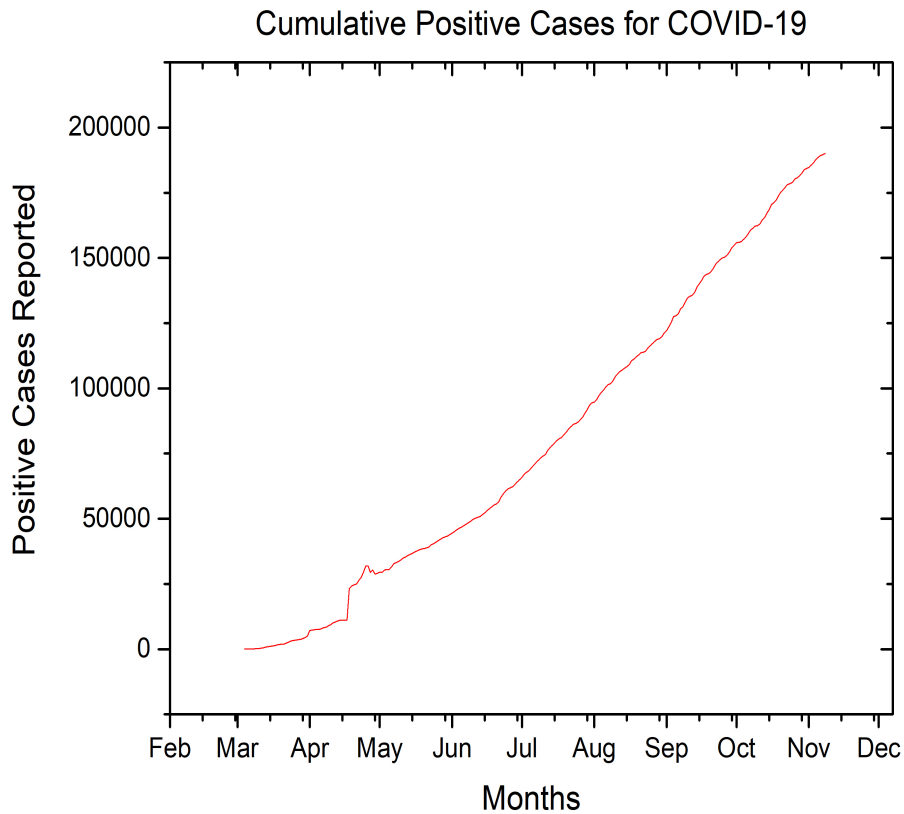


Figure 7.2: Cumulative chart of positive reported cases to november 2020. Data retrieved from:[6, 72, 73]

### 7.2.2 Associated and confirmed fatalities related to COVID-19

Ecuador reported its first COVID-19 death on March 13<sup>th</sup>. Since then, the daily number has increased at a mean rate of 52.10. By November 17<sup>th</sup>, 8,681 cumulative COVID-19 confirmed deaths were reported, and an additional of 4,344 deaths possibly were related to the disease,<sup>6</sup> resulting in an amount of 13,025 deaths. Although the mean number of reported deaths has remained relatively constant since March 14<sup>th</sup> - April 26<sup>th</sup>, the daily rate of reported deceases has progressively increased from 36.33 during this period to 133.73 during April 26<sup>th</sup> - May 11<sup>th</sup>. Since this last date, the mean death rate remains



positive, with a registered value of 50.16 cases per day. The cumulative values can be observed in figure 7.3, showing inaccuracies in some periods, in which the death rate could be observed as negative or even discontinuous.

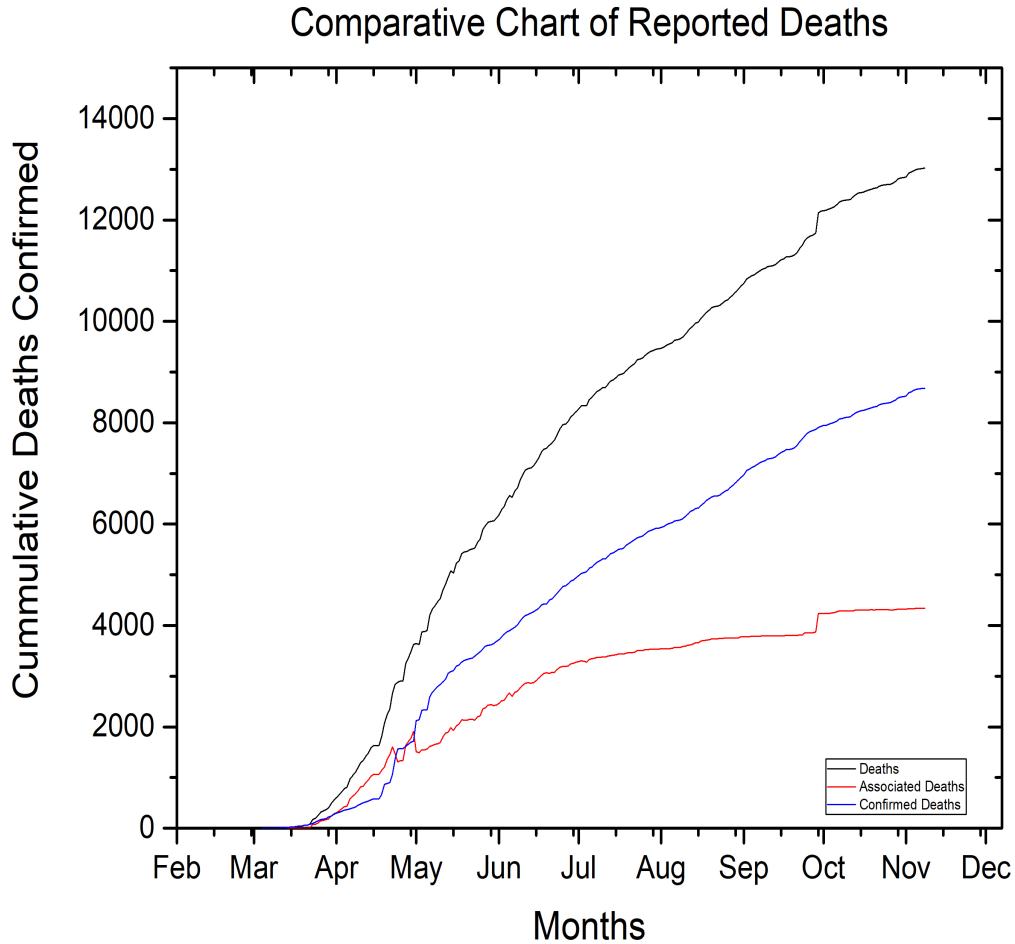


Figure 7.3: Cumulative daily confirmed and related deaths to COVID-19 disease. Data retrieved from online database: [6, 72, 73].

Both contributions to the number of deaths, from deaths of individuals with a confirmed diagnosis, and deaths related to the disease, as occurred by differentiating medical attention and lack of medicine, are presented in figure 7.4. This figure is evident not just in the hundreds of deaths caused by the COVID epidemic but the complex behavior that the recovered data exhibits.

From *Registro Civil del Ecuador and Centro de Operaciones de Emergencia* database of

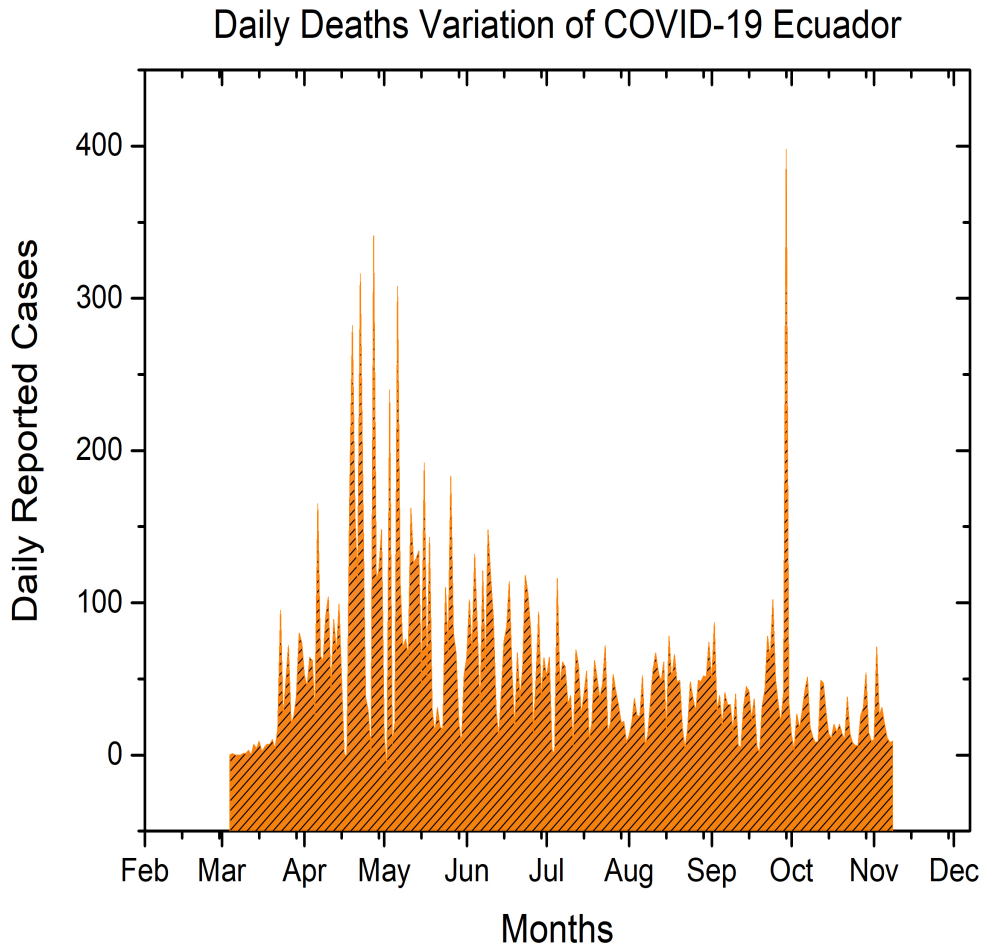


Figure 7.4: Cumulative daily deaths confirmed and related to COVID-19 disease. Data retrieved from online database: [6, 72, 73]

reported deaths from 2015 to 2020,<sup>6,73</sup> a historical-comparative chart is obtained and shown in figure 7.5. This comparison allows us to estimate the excess of deaths during the period in which the epidemic occurred. It is observed an increase of deaths in 2020, compared with previous years, and the pattern observed for 2020 closely matches the infected cases' behavior. For the data shown for 2020, it is observed a notable peak around April - May period. Coincidentally, this period reflects the large number of infected cases and deaths suffered by Guayaquil population during the COVID-19 epidemic. This city is one of the most populated of Ecuador, belonging to the province with the largest population, that is 2,7 million approximately.<sup>6</sup> It should be mentioned that other peak presented in the figure,

served in April 2016, is associated with the earthquake that hits the coast of Ecuador.

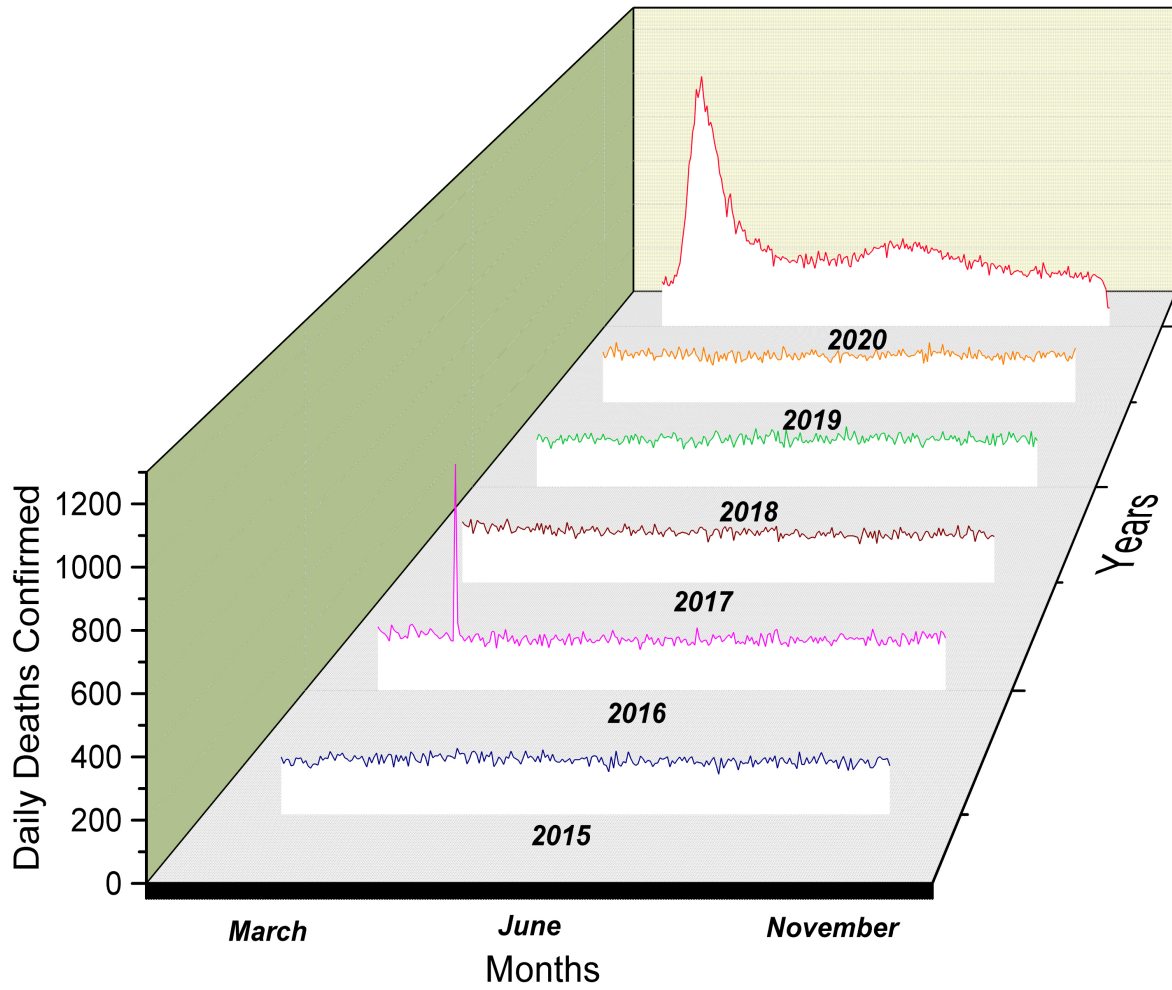


Figure 7.5: Historical Comparative Chart of cumulative deaths from March to November period. Data retrieved from online database: [6, 72, 73]

According to the presented data, it is crucial to consider that perceived incongruities compare with the number of deaths reported by the government. Even though the data plotted and shown in 7.5 refers to all deaths in Ecuador, regardless of their cause, the different pattern exhibited by the curve corresponding to the year 2020 compared to previous years presents the suspicion of a possible incidence of the COVID epidemic on the recorded data. This type of divergence between the reported data affects the strategies proposed to develop the analysis of the epidemic through the respective models. In any case, it is vital to observe that the pandemic outbreak directly influences the statistical behavior

of the recorded data, which constitutes an essential factor to consider in decision-making policies.

## 7.3 Forecasting COVID-19 epidemic dynamics through SIR and SEIR simulations.

### 7.3.1 SIR MODEL

In order to evaluate epidemic breakout through the SIR model, the transmission and recovery rates, denoted by  $\beta$  and  $\gamma$ , respectively, are obtained employing the equations 6.13 and 6.17 proposed by Bagal,<sup>71</sup> using the database published by governmental agencies and research groups,<sup>6,72,73</sup> shown in figure 7.2. The graphs resulting from the function given by the equation 6.13, applied to each temporal partition indicated in the table 7.1, are shown in figures 7.6 and 7.7, from which an approximately linear dependence of  $\ln(I)$  vs.  $t$  is observed. Here,  $I$  corresponds to the infected individuals' population in a given time  $t$ . The slope associated with each function in each temporal partition is reported in the table 7.2. On the other hand, the estimation of the  $\gamma$  parameter was reached by using the equation 6.17 for each defined temporal period, and once knowing  $m$  (slope linear regression) and  $\gamma$  values,  $\beta$  parameters were calculated, and they are also indicated in the table 7.2.

Table 7.2: Estimation of transmission ( $\beta$ ) and recovery ( $\gamma$ ) rates and basic reproductive ratio ( $R_0$ ) determined by using retrieved data for COVID-19 in Ecuador.

Kinetic parameters for COVID-19 data in Ecuador.				
Code	Period of time	$\beta$	$\gamma$	$R_0$
LD-0-1	March 13 <sup>th</sup> - March 23 <sup>th</sup>	0.44	0.05	8.79
LD-0-2	March 24 <sup>th</sup> - April 11 <sup>th</sup>	0.15	0.06	2.65
LD-0-3	April 12 <sup>th</sup> - April 26 <sup>th</sup>	0.12	0.08	1.44
CP-1	April 27 <sup>th</sup> - June 1 <sup>st</sup>	0.18	0.05	3.60
LD-2	June 6 <sup>th</sup> - Sept. 13 <sup>th</sup>	0.12	0.03	4.47
LD-3	Sept. 14 <sup>th</sup> - Nov. 11 <sup>th</sup>	0.11	0.04	2.52

From the values shown on table 7.2 can be appreciated that the transmission rate ( $\beta$ ) significantly decreases from the value for the initial partition with a bit of variance on CP1 due to previously exposed incongruousness in data. In contrast, the recovery rate ( $\gamma$ ) varies slightly. The changes observed in the transmission rate for the different temporal partitions seem to be directly related to the policies implemented by the Ecuadorian government and indicate the changes in the period of oscillation of the disease, making it challenging to analyze. From March 23 onwards, the transmission rate is continuously reduced. The government then advised, possibly as restriction policies, such as stay (and work) at home, closed schools, and banned most private and public events, begin to take effect. The implemented lockdown changed not only the probabilities of transmission per contact ( $\beta$ ) but also the contact patterns between susceptible and infectious individuals.

On the other hand, the slight variation on the recovery factor  $\gamma$  can be related to the capacity of the health system to give effective treatments and the implemented policies about the management of infected individuals. At the same time, the vaccine for the disease is not yet accessible. It is important to remember that  $\gamma$ , the recovery rate, is the inverse of the average infectious period and although sometimes it could be considered a constant value, most realistic representations take into account a dynamic behavior of this parameter.<sup>23,74</sup> Once determined  $\beta$  and  $\gamma$ , the basic reproductive ratio  $R_0$  can be found for each period considered. The  $R_0$  values estimated for each temporal period show erratic

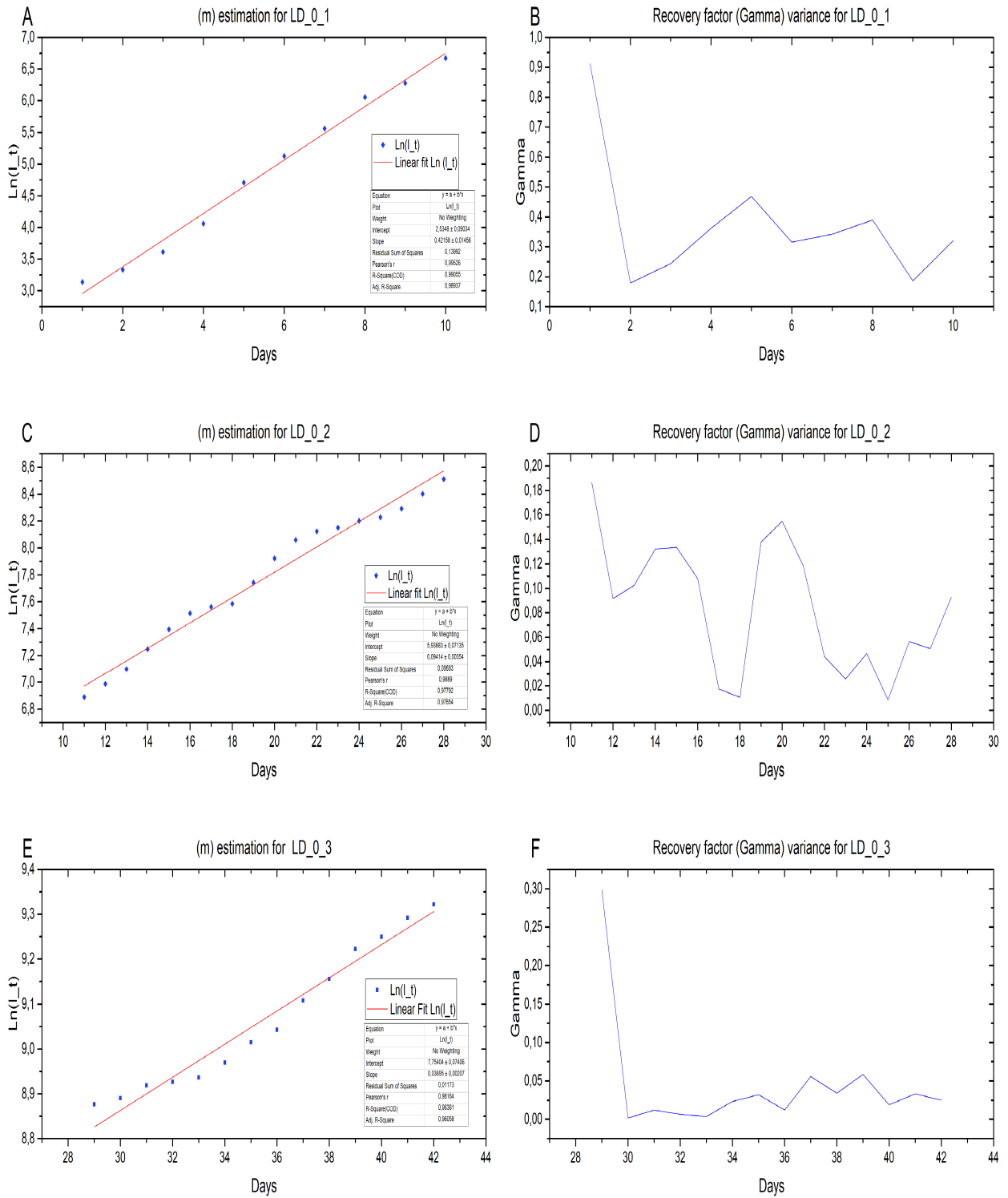


Figure 7.6: Left: Linear regression of the function  $\ln(I)$  vs.  $t$  for the first three temporal partitions: LD-01 (A), LD-02 (C), LD-03 (E), from which the relation between kinetic parameters associated with COVID-19 epidemic are determined from the slope  $m$  estimated for each regression. Right: Recovery rate ( $\gamma$ ) as a function of the time for the first three temporal partitions: LD-01 (B), LD-02 (D), LD-03 (F).

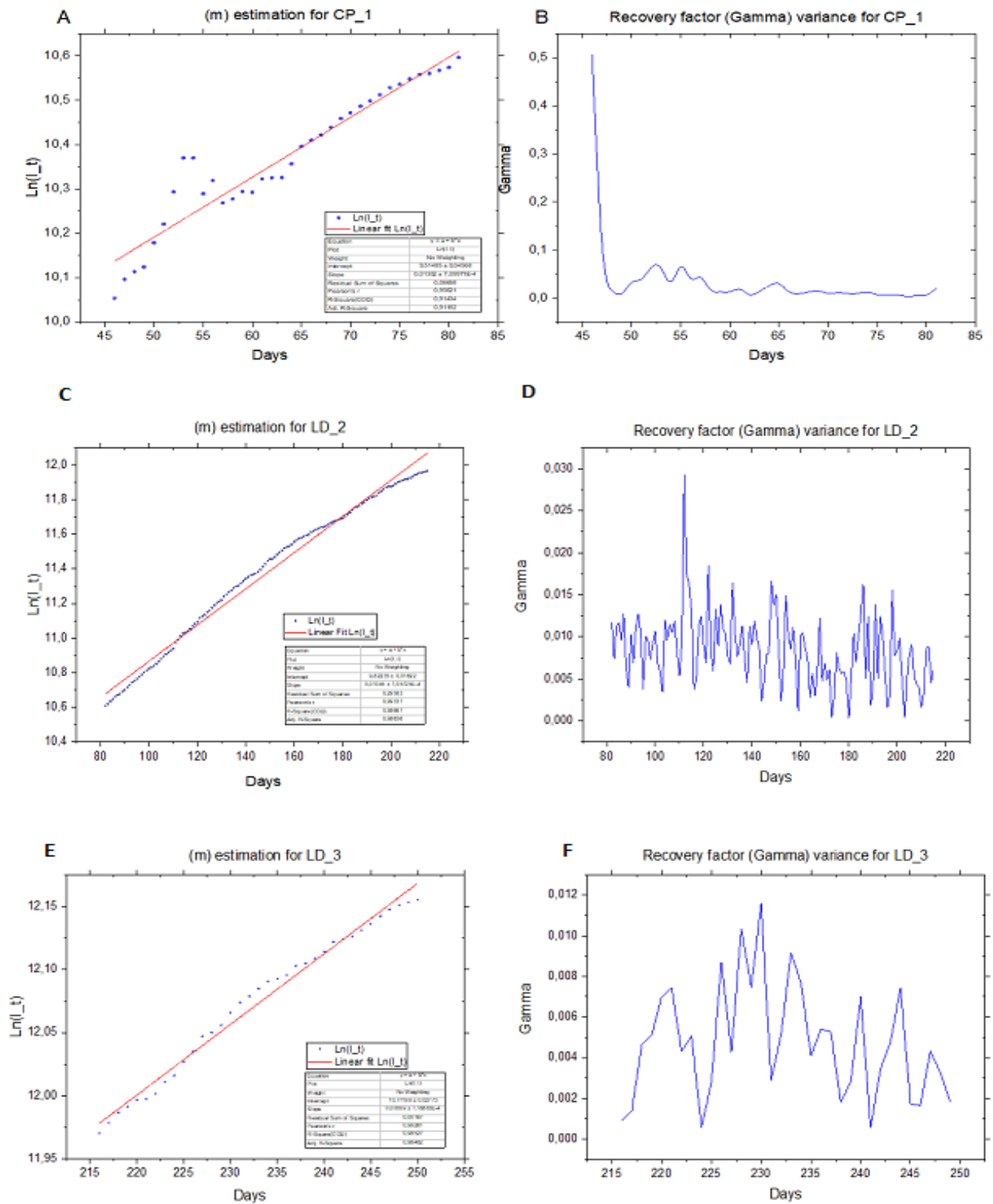


Figure 7.7: Left: Linear regression of the function  $\ln(I)$  vs.  $t$  for the last three temporal partitions: CP-1 (A), LD-2 (C), LD-3 (E), from which the relation between kinetic parameters associated with COVID-19 epidemic are determined from the slope  $m$  estimated for each regression. Right: Recovery rate ( $\gamma$ ) as a function of the time for the last three temporal partitions: CP-1 (B), LD-2 (D), LD-3 (F).

behavior, having the highest value for the first temporal partition at the beginning of the pandemic. Then, it tends to decrease due to the implementation of restrictive policies. However, as the partial curfew policies are implemented from June, the transmission rate increases to another high value. Finally, the low value obtained for the last period (LD-3: September-November) denotes a decrease in the transmission rate, and therefore in the  $R_0$  factor. Figure 7.8 shows the variation of the  $R_0$  factor for the different periods considered.

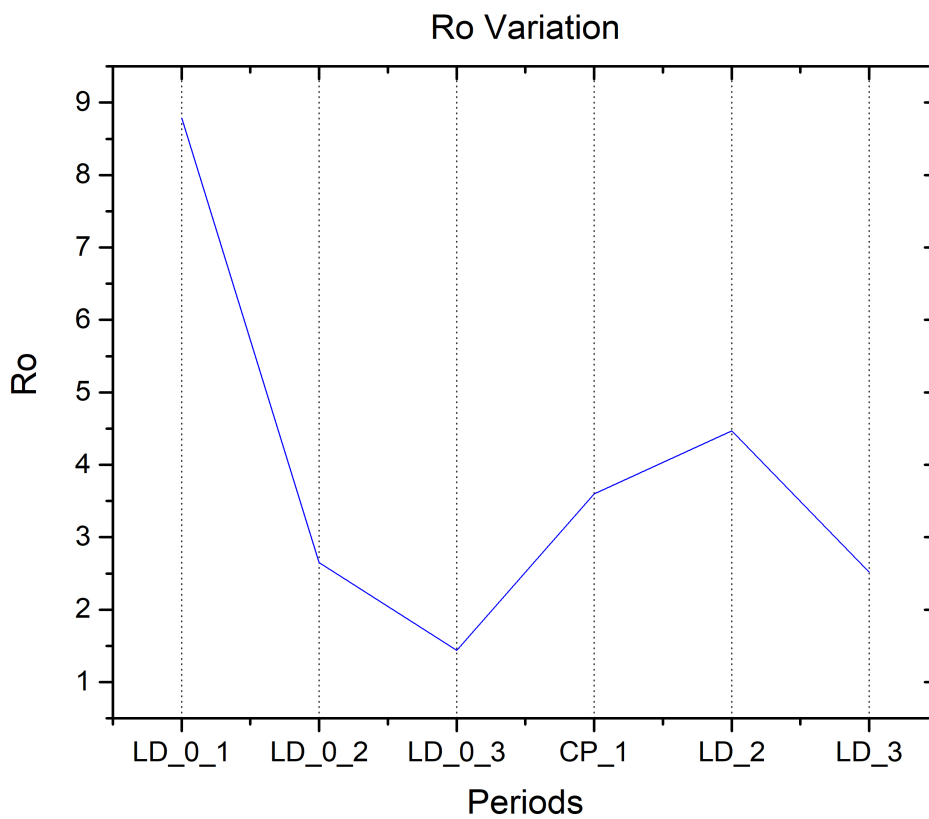


Figure 7.8: Variation of basic reproductive ratio ( $R_0$ ) through temporal periods considered.

Due to the very narrow variation of the estimated values for  $\gamma$ , and the fact that the SIR model assumes a constant value for this parameter, an average value was obtained from the different results for *gamma* reported in the table 7.2. The average value corresponds to  $\gamma = 0.052 \pm 0.006$ , which agrees with the most frequently reported value for  $\gamma$ .<sup>75</sup> With this average value for  $\gamma$ , new values for  $R_0$  factor were determined, and they are shown in



the table 7.3, among the other kinetic parameter for each temporal periods defined. The  $\beta$  values were not changed due to their significant variation in the different temporal periods. From the values reported for kinetic parameters, the simulations of SIR and SEIR models were carried out, representing the temporal evolution of the population of susceptible (S), infected (I), Exposed (E), and recovered (R) individuals during the considered period of COVID-19 epidemic.

Table 7.3: Kinetic parameters associated to COVID-19 epidemic in Ecuador: transmission ( $\beta$ ) and average recovery ( $\gamma$ ) rates and re-normalized basic reproductive ratio ( $R_0$ ), determined by using official retrieved data reported in Ecuador.

Re-normalized kinetic parameters for COVID-19 data in Ecuador .				
Code	Period of time	$\beta$	$\gamma_n$	$R_0$
LD-0-1	March 13 <sup>th</sup> - March 23 <sup>th</sup>	0.44	0.052	8.79
LD-0-2	March 24 <sup>th</sup> - April 11 <sup>th</sup>	0.15	0.052	3.03
LD-0-3	April 12 <sup>th</sup> - April 26 <sup>th</sup>	0.12	0.052	2.43
CP-1	April 27 <sup>th</sup> - June 1 <sup>st</sup>	0.18	0.052	3.60
LD-2	June 6 <sup>th</sup> - Sept. 13 <sup>th</sup>	0.12	0.052	2.40
LD-3	Sept. 14 <sup>th</sup> - Nov. 11 <sup>th</sup>	0.11	0.052	2.20

### 7.3.2 SIR model simulation for LD-0-1: $\beta = 0.44$ , $\gamma = 0.052$ , $R_0 = 8.79$

In figure 7.9 are shown the results for differential equations associated to the SIR model, given by the equations 6.1 - 6.3, taking into account the kinetic parameters ( $\beta$ ,  $\gamma$  and  $R_0$ ) values previously determined and depicted in table 7.3. The curves shown in figure 7.9 corresponds to the stochastic evaluation of data retrieved during the period between March 13<sup>th</sup> and March 23<sup>th</sup>, period remarked as the beginning of the curfew policies. The exponential increase of the infected population, represented by the red curve, after 50 days from the report of the first COVID-19 case on Ecuador, reaching a maximum value, identified as a critical point, on the range from 50 to 65 days (between April - May). It should be noted that this time range coincides with the events situated in Guayaquil, on

the period April 23<sup>th</sup> - May 11<sup>th</sup>, during which the region experienced a large increase in the number of infected individuals. According to the curve ( $I$  vs.  $t$ ), at this point, around 64 % of the total population get infected with COVID-19, the corresponding population of 11.7 million. The temporal evolution of recovered individuals represented by the green curve shows a rapid increase from 50 to 120 days. The rapidly recovered phenomena are explained by the number of people infected, and the low mortality rate due to the disease, estimated around 0.5-1, according to the data reported.<sup>76</sup> The blue curve represents the temporal variation of the susceptible population, being consistent with the expected behavior.

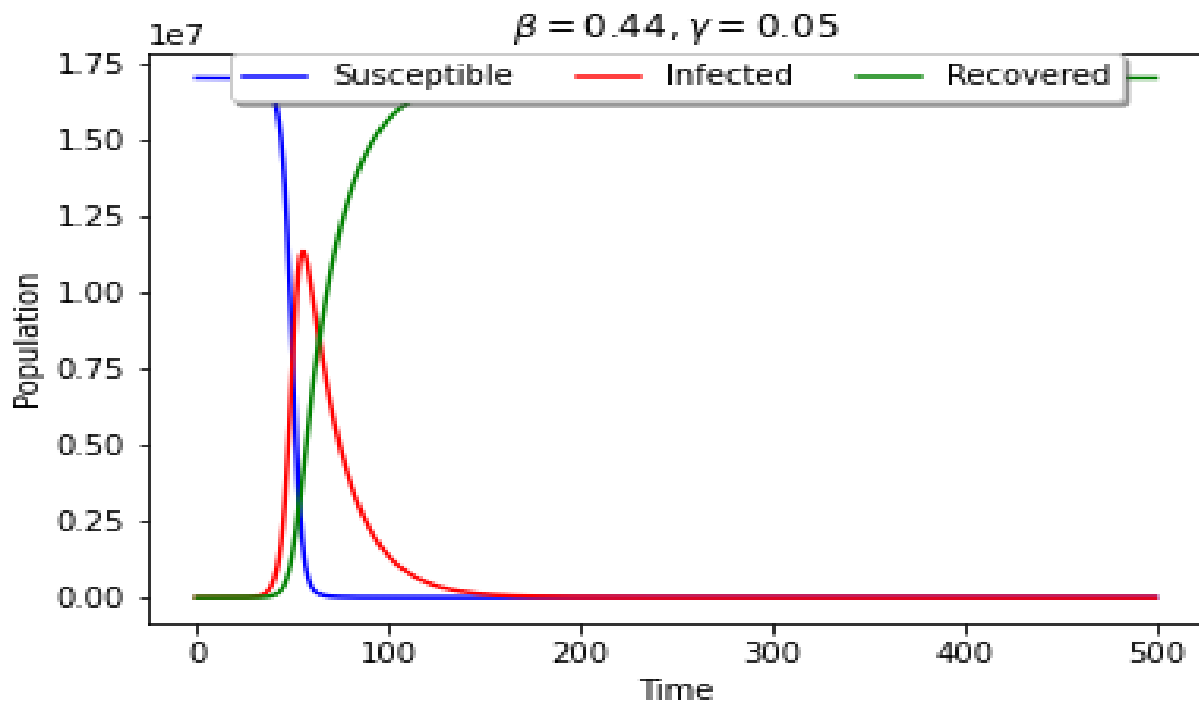


Figure 7.9: Results for SIR model for temporal period LD-0-1:  $\beta=0.44$   $\gamma=0.052$  and  $R_0=8.79$ . Initial Ecuadorian susceptible population: 17,000,000

Evaluating this period with the average fatality rate of Ecuador 5.43,<sup>57</sup> representing a deceased population of 635,310. The entire range of time in which is evidenced variation of susceptible, infected, and recovered population is up to around August 20<sup>th</sup>, assuming this date as the ending of the first epidemic wave, according to SIR model with the kinetic parameters established. This period can be related to the dynamics of the first wave of the COVID-19 epidemic in Ecuador. Qualitatively, the behavior of curves shown in figure 7.9

has similarity with those shown in figure 2.1, corresponding to the temporal evolution of chemical species during a reaction mechanism of two steps involving intermediate species. The correspondence in this analogy is compatible with: reactant species  $\rightarrow$  susceptible individuals (blue curve), intermediate species  $\rightarrow$  infected individuals (red curve), and product species  $\rightarrow$  recovered individuals (green curve). Such similarity implies that the rate constant for the first step, intermediate species formation, is much higher than the rate constant for the second step, intermediate species consumption, understood as  $\beta > \gamma$ . This assumption is for this first temporal period, consistent with the obtained results.

### 7.3.3 SIR model simulation for LD-0-2: $\beta = 0.15$ , $\gamma = 0.052$ , $R_0 = 3.03$

Now, the simulation for the second temporal period considered (LD-02) results in curves depicted in figure 7.10, which correspond to the stochastic evaluation of time variation of S, I, and R individuals during the period between September 24<sup>th</sup> - October 12<sup>th</sup>. For this period, values obtained for the  $\beta$  and  $R_0$  differ concerning those used for the previously evaluated period, while the  $\gamma$  value is the same.

In this period, the effects of the curfew policies implemented by government agencies, such as social distancing, permanent face masks, restricted movement of citizens, start to be reflected on the temporal evolution of S, I, and R individuals population. The maximum observed for the curve corresponding to infected individuals (red curve) is displaced on time and is flattened compared to the curve depicted in figure 7.9. The total amount of infected cases diminish to around 5.3 million of cases which indirectly means an estimated death toll of 287,779. The behavior of the curves corresponding to susceptible and recovered individuals, blue and green curves, respectively, are also changed concerning the previous period evaluated, exhibiting a displacement to higher times and a slow increase. These changes exhibited are consistent because restrictive policies are taking effect, even more so when one of them involved curfew.

By comparison with the analog curves for a chemical reaction (figure 2.1), the situation of a higher speed constant for the first process is maintained, that is,  $\beta > \gamma$ . However, a

lower sharpness of the peak for the temporal evolution of infected individuals is observed and a more gradual change for the temporal evolution of susceptible and recovered individuals. These differences could be a consequence of a lower difference between both rate constant, that is, between  $\beta$  and  $\gamma$ .

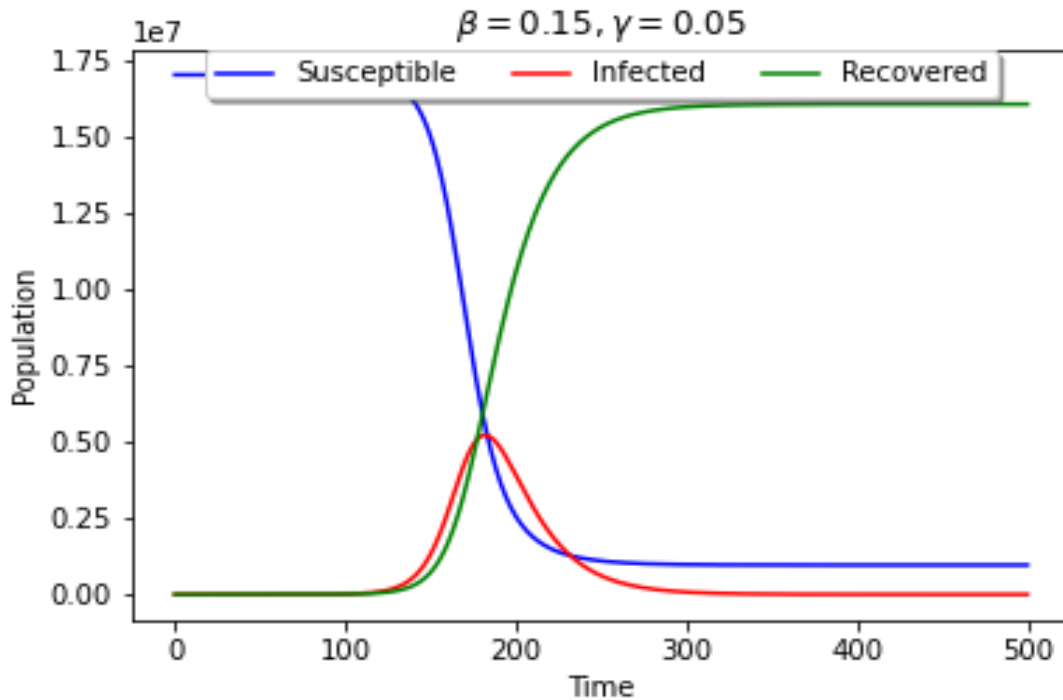


Figure 7.10: Results for SIR model for temporal period LD-0-2:  $\beta=0.15$   $\gamma=0.05$  and  $R_0=3.03$ . Initial Ecuadorian susceptible population :16,999,465.

### 7.3.4 SIR model simulation for LD-0-3: $\beta = 0.12$ , $\gamma = 0.052$ , $R_0 = 2.43$

For this temporal period, with different values for  $\beta$  and  $R_0$ , the peak of the curve representing the variation in time of infected individuals population is again displaced, this time approximately day 250 (between November 10-November 20). The value of infected individuals, at this point, corresponds to an amount of 4.2 million. The death toll estimated is around 228,060 cases, using the average value of the fatality rate for Ecuador reported by OurWorldinData.org<sup>57</sup>

Both the displacement of the red curve, corresponding to the temporal evolution of the infected individuals, and its flatness suggest that the infectious wave ends without infecting all the susceptible individuals, due to the low spread of the virus reached by the restrictions in the mobility, programmed curfew, permanent mask, and hygiene campaigns.

Again, a behavior of the curves similar to those presented in figure 2.1-a (higher rate constant for the first process) is observed, but with more excellent proximity to the behavior of figure 2.1-b, but without reaching it.

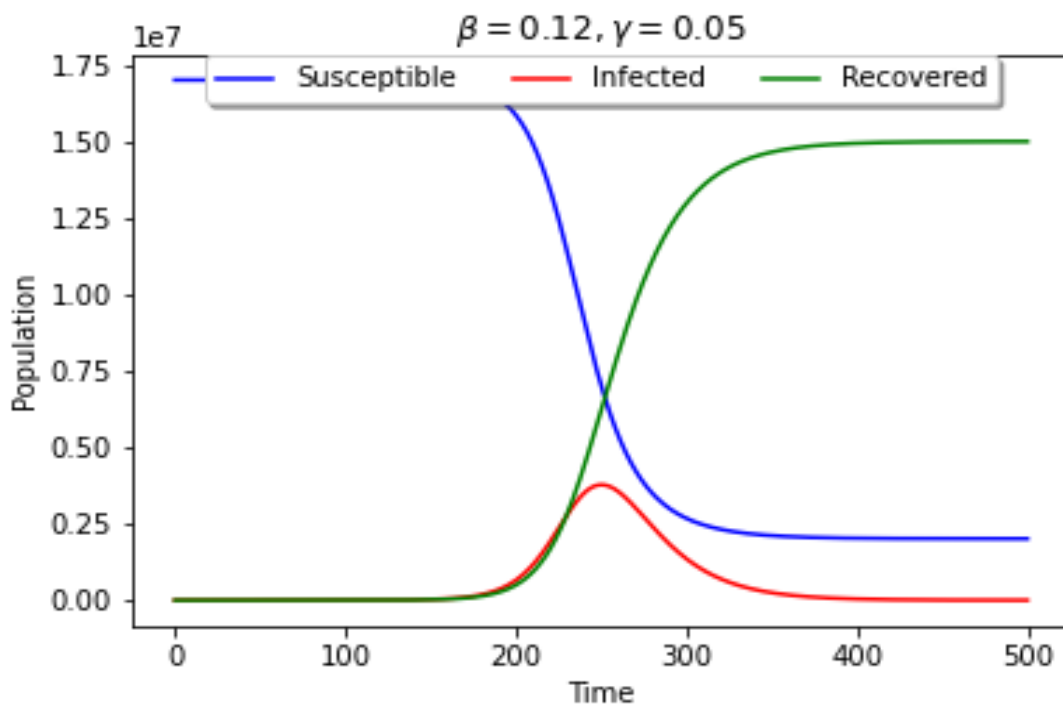


Figure 7.11: Results for SIR model for temporal period LD-0-3:  $\beta=0.12$   $\gamma=0.05$  and  $R_0=2.43$ . Initial Ecuadorian susceptible population: 16,995,410.

### 7.3.5 SIR model simulation for CP-1: $\beta = 0.18$ , $\gamma = 0.052$ , $R_0 = 3.60$

The critical point period is characterized by inaccuracies in reported data for the infected individuals diagnosed. Results for simulation of SIR model are depicted in figure 7.12, shown a shift of the maximum of the curve to earlier times at the beginning of the epidemic,

located at a time less than day 200, approximately at day 150. This behavior indicates that disease is gaining presence again in the population. The red curve has a remarkable sharpness again, and the value of maximum corresponds to an amount of positive infected cases of approximately 6,7 million. The number of deaths is very similar to that which resulted from the analysis of figure 7.10, which is 363,810, which could indicate disease resilience. The low respect to the general population's anti-pandemic policies, related to the tiredness and fatigue that the pandemic situation, and the restrictions imposed, has generated in society, may also be responsible.

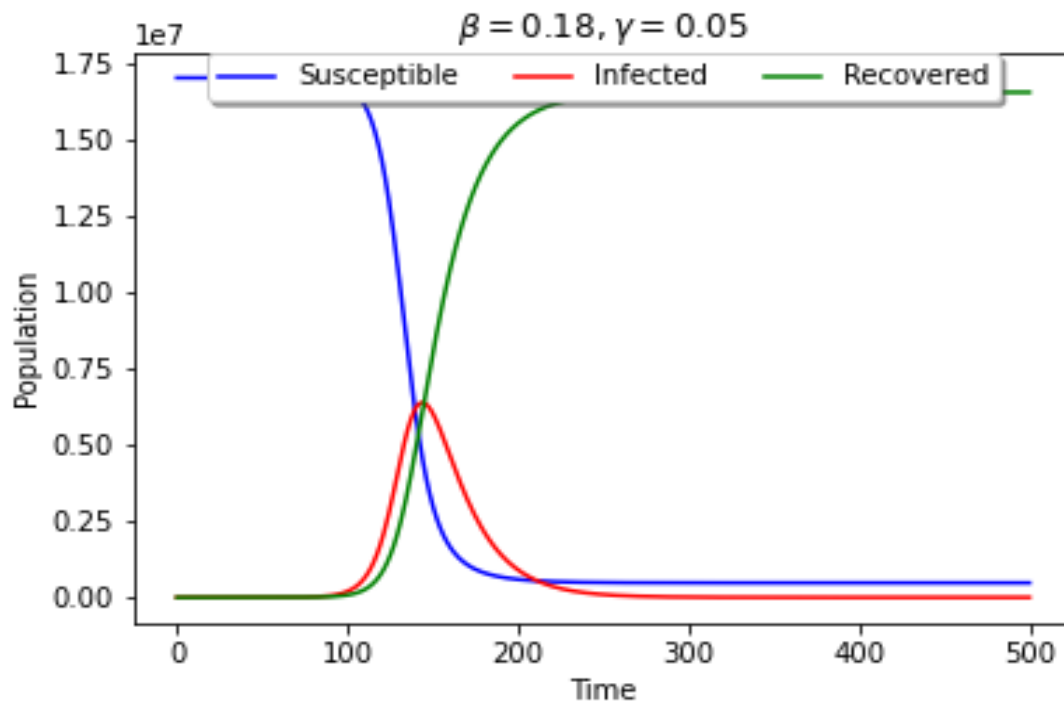


Figure 7.12: Results for SIR model for temporal period CP-1:  $\beta=0.18$   $\gamma=0.052$  and  $R_0=3.60$ . Initial Ecuadorian susceptible population: 16,995,410.

### 7.3.6 SIR model simulation for LD-2: $\beta = 0.12$ , $\gamma = 0.052$ , $R_0 = 2.40$

Figure 7.13 corresponds to results for simulation SIR model for the period between June 2<sup>th</sup> - September 13<sup>th</sup>. The shift of the maximum of the infected individuals (red curve) occurs

at day 250, indicating an increase in the dynamics of the disease spread. It is important to remark that, during this period, some curfew policies were partially removed, and, in consequence, factors as mobility and human interaction could be responsible to facilitates the disease transmission.<sup>77</sup> The infected individuals increased to a value of around 4,5 million in November 2020, and a denoted recovery curve can be observed in a short period (high pressure on the medical care system). The death toll for this period is approximately 248,652 and, the end of the wave is estimated on January- February 2021.

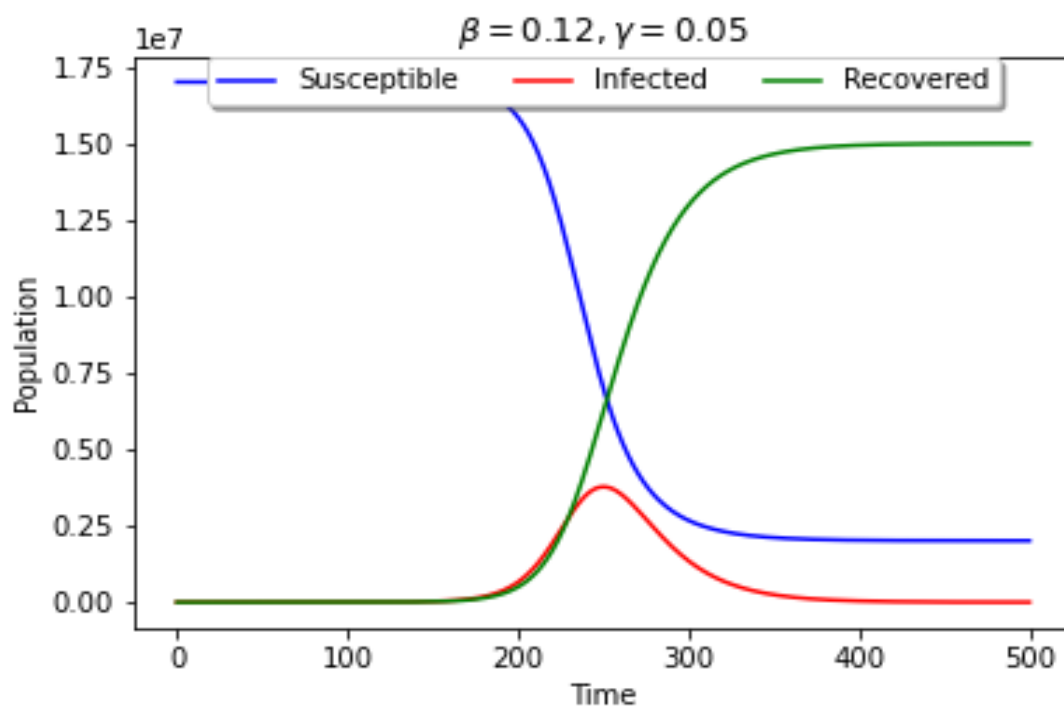


Figure 7.13: Results for SIR model for temporal period LD-2.  $\beta=0.12$   $\gamma=0.05$  and  $R_0=2.40$ . Initial Ecuadorian susceptible population: 16,987,451.

### 7.3.7 SIR model simulation for LD-3: $\beta = 0.11$ , $\gamma = 0.052$ , $R_0 = 2.20$

Chart 7.14 shows a decrease on the infected peak and a pronounced displacement over time. Many factors could be affecting the pandemic at this point. At first, the number of infected cases is high compared to the start of the pandemic, which means a decrease

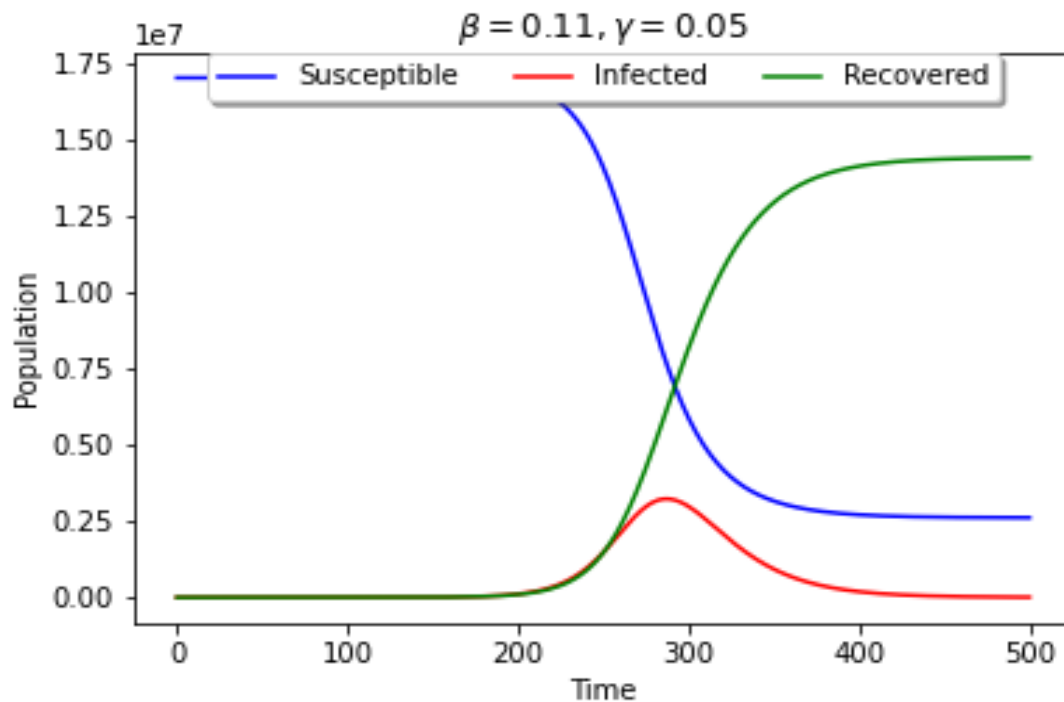


Figure 7.14: Results for SIR model for temporal period LD-3.  $\beta=0.12$   $\gamma=0.05$  and  $R_0=2.20$ . Initial Ecuadorian susceptible population: 16,955,386.

in the number of susceptible populations. Second, the asymptomatic population gain quickly immunity against the disease which also represent a fewer impact of the disease on susceptible. The peak for this period is reached on day 290 (July 2021) with approximately 3.8 million people infected with the disease. Notice that the infected curve flattens on day 350 before infecting all susceptible on country. At this point, healthcare system will have more efficiency in given treatment to the severe cases which is reflected in the amount of deaths estimated, which is: 206,343 cases approximately.



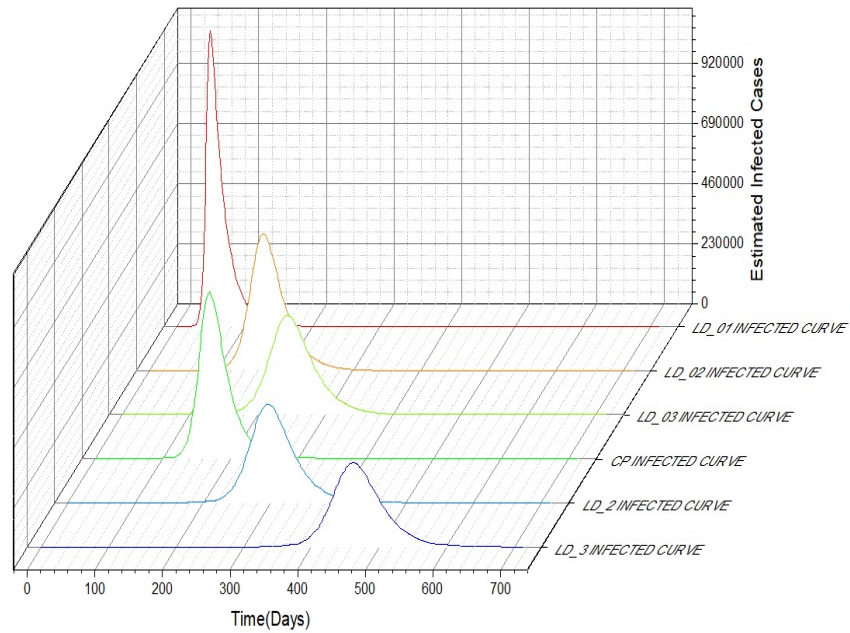


Figure 7.15: Comparative chart of COVID-19 infected curve peak from established periods

Chart 7.15 is a general representation of the spread of COVID-19 disease in Ecuador. This estimation is made by combining each of the infected peak curves retrieved from SIR model. The combination of the data allows recreating a possible scenario in Ecuador over two years COVID-19 pandemic in where the peaks reflect the possible dates at which the disease will be "out of control." Furthermore, it shows the flatten phenomena on curves over time due to the implementation of curfew policies by local government. It is remarkable to notice that the values for CP-1 and LD03 show a similar curve over time. This situation occurs due to the issues in the data previously mentioned during this period.

### 7.3.8 SEIR MODEL

To perform SEIR model evaluation is necessary to consider the values retrieved for the SIR model on table 7.3 and a set of specific epidemiological values related to COVID-19 disease. These values were retrieved from literature<sup>75,78</sup> given the following table:

SEIR Model Parameters	
population	1,70E+07
incubation_period	5,68
infectious_period	4,92
initial_R0	2,74
hospitalization_probability	0,21
hospitalization_duration	17,7
hospitalization_lag_from_onset	10
icu_probability	0,05
icu_duration	17,7
icu_lag_from_onset	9,84
death_probability	0,02
death_lag_from_onset	15,93
population_exposed	0,001
population_infected	0,001

Figure 7.16: SEIR model configuration values.

In contrast to SIR model, SEIR model allows adding parameters that increase the precision of the model, such as incubation period, hospitalization probability, need of intensive care unit (ICU) probability, and death probability (duration and delay in days). This situation allows predicting the spread of the disease and acute when the healthcare capacity will be overwhelmed. Also, the SEIR model allows the generation of large models without dividing the data into different periods. For this reason, a median of  $\beta$  and  $\gamma$  from Ecuador data were selected giving a  $R_0$  median of 2.74.

Figure 7.17 is an SEIR model of COVID-19 spread in Ecuador. Here many peaks corresponding to the exposed, infected (active), hospitalized (active), ICU, and deaths are observed. The infected curve shows a rapid increase with a significant peak registered at days 50-70 from the beginning of the epidemic breakout. In terms of dates the peak is between April and May and shows an average 2 million of people infected. The exposed curve is closely related to the infected curve because it represents an estimation of the

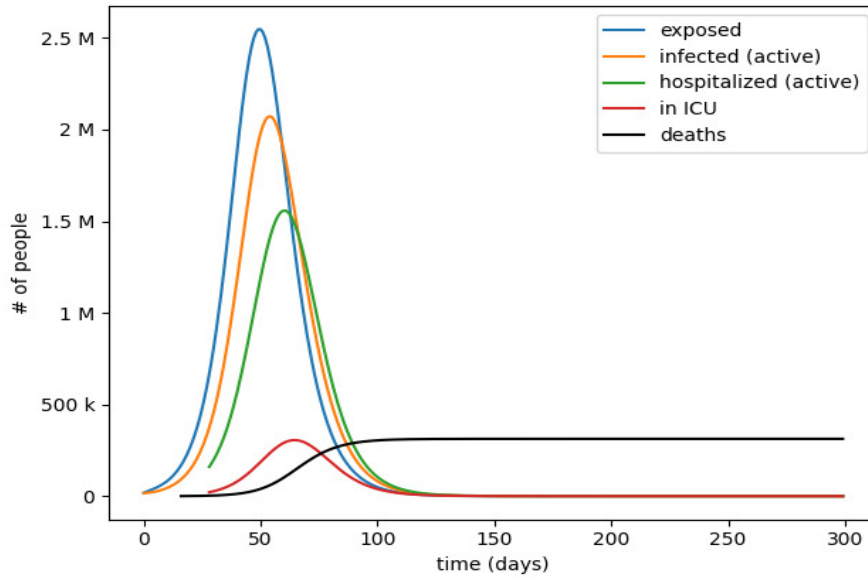


Figure 7.17: SEIR Chart.  $R_0=2.74$ . Probabilities: Hosp:0.21, ICU:0.05 Death:0.02. Ecuadorian Population Susceptible considered:17000000

possible interaction between infected cases and susceptible remains. Chart 7.17 represents the prominent peak observed with an average of 2.5 million exposed. Notice that the peak is located before the other peaks (between 50-60 days), indicating a delay between the reported cases and the probably exposure. The other peaks observed in the chart correspond to the hospitalization, ICU, and deaths. The hospitalized peak is based on the probability of an infected case that needs specialized treatment and occurs after the peak of infected cases between 60-80 days. The value showed by the chart shows an amount of 1.5 million people hospitalized, which widely exceeds the capacity of the Ecuadorian health care system (23.803 beds for moderate cases<sup>79</sup>). The peak for severe cases (in ICU) also overcomes the available amount of ICU units (1183 in all healthcare systems<sup>79</sup>) with an average of 300000 cases. This peak will be reached simultaneously with the hospitalized peak, putting more stress on the healthcare system. The deaths predicted will reach an amount of 300000 cases by day 90 (June 2020).

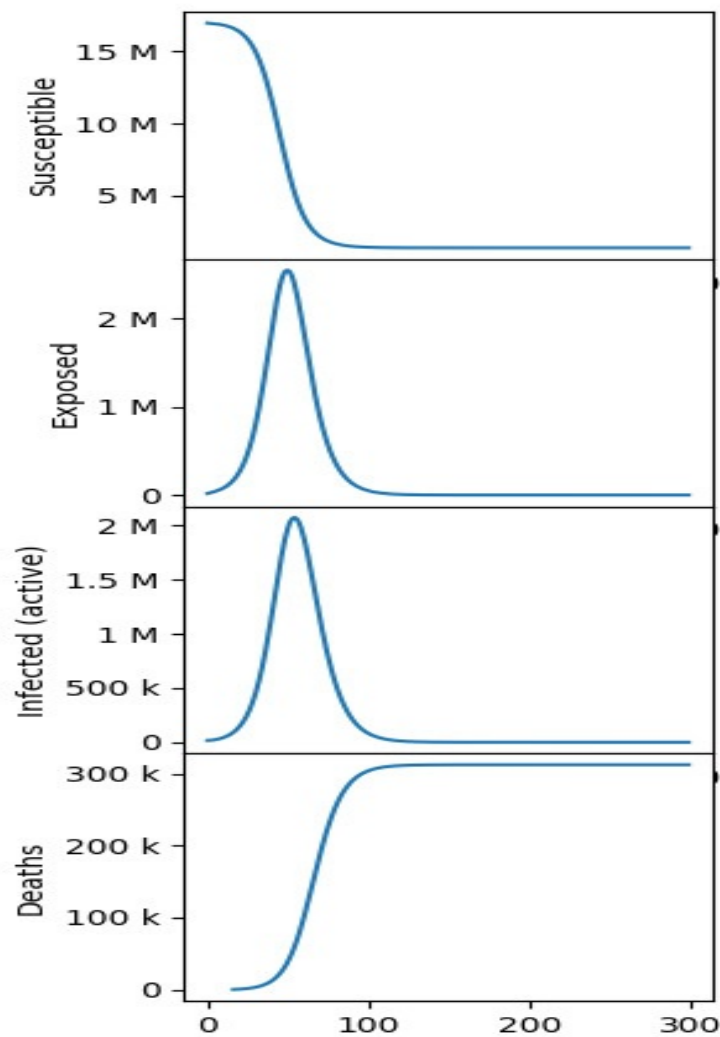


Figure 7.18: Amplified curves of Susceptible, Exposed, Infected and Deaths related to SEIR model

Figure 7.18 shows a more detailed view of the peaks obtained by the model. Here is more easy to observe the average estimation of cases for each of the curves obtained with the SEIR model. Notice that the model does not show the number of recovered cases and has a singular behavior after 100. This behavior is related to the lack of a demographic and mobility information (contact matrix) for the Ecuadorian population and dispersion of CFR (Fatality rate) between ages of biological sex structures. These factors add an essential enhancement of the modeling, allowing predicting the spread for a longer time-widespan.

# Chapter 8

## Conclusions

This work introduces a compartmental SIR and SEIR model describing temporal propagation of disease contagion and applied it to the 2020 outbreak of COVID-19 in Ecuador. Our simulations are intended to provide a proof-of-concept of the potential of SIR and SEIR models for regional modeling of the outbreak. Nonetheless, they show good qualitative agreement with reality, accurately predicting the outbreak dynamics and recreating the transmission path in time. The SIR and SEIR kinetic models are used to examine some possible reopening scenarios, which suggested that reopening may be best determined based on local population and contagion dynamics. However, when accurately predicting the number of infected dead or recovered, it had a great difference with official data given by COE. These phenomena may occur due to the country's inefficiency to take and process patient samples in an orderly fashion, a low detection rate of asymptomatic patients, a high percentage of false negatives and false positives and fatalities not recorded. The uncertainty in our predictions is considered large because of several unknown reasons arising from: model assumptions, population demographics, the number of COVID-19 diagnostic tests realized per day, contact matrix, testing criteria, the accuracy of the test results, and heterogeneity in implementation of different government-initiated interventions and community-level protective measures across the country. Furthermore, the models do not consider the age structure, contact patterns, or spatial information in order to refine the predictions. It is important to consider that COVID-19 hotspots in Ecuador are not uniformly spread across the country, and state-level forecasts may be

more meaningful for state-level policymaking. The models proposed simulates the outbreak for the whole nation. In consequence, in-country variations might exist. It suggested that similar approaches should be made at a local scale. Regardless of the caveats in our study, our analyses show the impact and necessity of lockdown and suppressed activity post-lockdown in Ecuador.

# Bibliography

- (1) Simon, C. M. *The SIR dynamic model of infectious disease transmission and its analogy with chemical kinetics*. *PeerJ Physical Chemistry* **2020**, DOI: 10.7717/peerj-pchem.14.
- (2) Engel, T.; Reid, P., *Thermodynamics, Statistical Thermodynamics, & Kinetics*, 2013, pp 524–527.
- (3) Hao, T. Infection Dynamics of Coronavirus Disease 2019 (Covid-19) Modeled with the Integration of the Eyring's Rate Process Theory and Free Volume Concept, 2020.
- (4) Keeling, M. J. *Models of foot-and-mouth disease*. *RSC* **2005**, DOI: 10.1098/rspb.2004.3046.
- (5) Kermack, O. W.; McKendrick, A. G. *Proceedings of the Royal Society of London. Series A, Containing Papers of a Mathematical and Physical Character* **1927**, DOI: 10.1098/rspa.1927.0118.
- (6) De Operaciones de Emergencia Nacional, C., *Informes de Situación COVID-19 Ecuador*. Online resource: <https://github.com/andrab/ecuacovid/tree/master/informes/SNGRE>, 2020.
- (7) Engel, T.; Reid, P., *Thermodynamics, Statistical Thermodynamics, & Kinetics*, 2013, pp 501–503.
- (8) Lund, E. W. Guldberg and waage and the law of mass action. *Journal of Chemical Education*, 1965.

- (9) Guldberg, C. M.; Waage, P. *Ueber die chemische Affinität. § 1. Einleitung. Journal für Praktische Chemie* **1879**, DOI: 10.1002/prac.18790190111.
- (10) Bagshaw, C. R. In *Encyclopedia of Biophysics*, Roberts, G. C. K., Ed.; Springer Berlin Heidelberg: Berlin, Heidelberg, 2013, pp 1233–1234.
- (11) Chung, P. Law of mass action, 2020.
- (12) Engel, T.; Reid, P., *Thermodynamics, Statistical Thermodynamics, & Kinetics*, 2013, pp 488–492.
- (13) Muller, P. *Glossary of terms used in physical organic chemistry: (IUPAC Recommendations). Pure and Applied Chemistry* **1994**, DOI: 10.1351/pac199466051077.
- (14) Keener, J. P.; Sneyd, J. *Mathematical Physiology* **2008**.
- (15) Atkins, P.; Paula, J. D. *Atkins' Physical chemistry* 8th edition, 2009.
- (16) Laidler, K. J.; King, M. C. *The development of transition-state theory. Journal of Physical Chemistry* **1983**, DOI: 10.1021/j100238a002.
- (17) Higgins, J. *the Theory of Oscillating Reactions - Kinetics Symposium. Industrial & Engineering Chemistry* **1967**, DOI: 10.1021/ie50689a006.
- (18) Viguerie, A.; Veneziani, A.; Lorenzo, G.; Baroli, D.; Aretz-Nellesen, N.; Patton, A.; Yankeelov, T. E.; Reali, A.; Hughes, T. J.; Auricchio, F. *Diffusion–reaction compartmental models formulated in a continuum mechanics framework: application to COVID-19, mathematical analysis, and numerical study. Computational Mechanics* **2020**, DOI: 10.1007/s00466-020-01888-0.
- (19) Blagojević, S.; Pejić, N.; Anić, S.; Kolar-Anić, L. *Belousov-Zhabotinsky oscillatory reaction. Kinetics of malonic acid decomposition. Journal of the Serbian Chemical Society* **2000**, *65*, 709–713.
- (20) Acrivos, J. *Physical chemistry. Journal of Chemical Education* **1988**, *65*, DOI: 10.1021/ed065pa335.3.
- (21) McQuarrie, D. A. *Stochastic approach to chemical kinetics. Journal of Applied Probability* **1967**, DOI: 10.2307/3212214.



- (22) Murray, J. D., *Mathematical Biology : I . An Introduction , Third Edition*, 2002.
- (23) Keeling, M. J.; Rohani, P., *Modeling Infectious Diseases through Contact Networks*, 2008, p 16.
- (24) Siettos, C. I.; Russo, L. *Mathematical modeling of infectious disease dynamics*, 2013.
- (25) Sy, C.; Ching, P. M.; San Juan, J. L.; Bernardo, E.; Miguel, A.; Mayol, A. P.; Culaba, A.; Ubando, A.; Mutuc, J. E. *Process Integration and Optimization for Sustainability* **2021**, DOI: 10.1007/s41660-021-00156-9.
- (26) Defra *Foot and mouth disease control strategy for Great Britain* **2011**, 34.
- (27) Meltzer, M. I.; Damon, I.; LeDuc, J. W.; Millar, J. D. *Emerging Infectious Diseases* **2001**, DOI: 10.3201/eid0706.010607.
- (28) Halloran, M. E.; Longini, I. M.; Nizam, A.; Yang, Y. *Science* **2002**, DOI: 10.1126/science.1074674.
- (29) Hao, T., *Electrorheological Fluids - The Non-aqueous Suspensions*, 2005.
- (30) Manenti, F.; Galeazzi, A.; Bisotti, F.; Prifti, K.; Dell'Angelo, A.; Di Pretoro, A.; Ariatti, C. *Chemical Engineering Science* **2020**, DOI: 10.1016/j.ces.2020.115918.
- (31) Lydeamore, M. J.; Campbell, P. T.; Price, D. J.; Wu, Y.; Marcato, A. J.; Cunningham, W.; Carapetis, J. R.; Andrews, R. M.; McDonald, M. I.; McVernon, J.; Tong, S. Y. C.; McCaw, J. M. *PLOS Computational Biology* **2020**, *16*, ed. by Kouyos, R. D., e1007838.
- (32) Anderson, R. M.; May, R. M., *Infectious diseases of humans: Dynamics and control*, 1992.
- (33) Gomes, M. G. M.; Gjini, E.; Lopes, J. S.; Souto-Maior, C.; Rebelo, C. *Journal of Theoretical Biology* **2016**, *395*, 97–102.
- (34) Diekmann, O.; Heesterbeek, H.; Britton, T., *Mathematical tools for understanding infectious disease dynamics*, 2012.

- (35) Nishiura, H.; Chowell, G. In *Mathematical and Statistical Estimation Approaches in Epidemiology*, 2009.
- (36) Lloyd-Smith, J. O.; Schreiber, S. J.; Kopp, P. E.; Getz, W. M. *Nature* **2005**, DOI: 10.1038/nature04153.
- (37) Weitz, J. S.; Dushoff, J. *Scientific Reports* **2015**, DOI: 10.1038/srep08751.
- (38) Viguerie, A.; Lorenzo, G.; Auricchio, F.; Baroli, D.; Hughes, T. J.; Patton, A.; Reali, A.; Yankeelov, T. E.; Veneziani, A. *Applied Mathematics Letters* **2021**, DOI: 10.1016/j.aml.2020.106617.
- (39) Horrox, R., *The black death*, 2013.
- (40) Trilla, A.; Trilla, G.; Daer, C. The 1918 "Spanish Flu" in Spain, 2008.
- (41) Pike, B. L.; Saylor, K. E.; Fair, J. N.; Lebreton, M.; Tamoufe, U.; Djoko, C. F.; Rimoin, A. W.; Wolfe, N. D. The origin and prevention of pandemics, 2010.
- (42) Worobey, M.; Gemmel, M.; Teuwen, D. E.; Haselkorn, T.; Kunstman, K.; Bunce, M.; Muyembe, J. J.; Kabongo, J. M. M.; Kalengayi, R. M.; Van Marck, E.; Gilbert, M. T. P.; Wolinsky, S. M. *Direct evidence of extensive diversity of HIV-1 in Kinshasa by 1960. Nature* **2008**, DOI: 10.1038/nature07390.
- (43) Guan, Y. et al. *Isolation and characterization of viruses related to the SARS coronavirus from animals in Southern China. Science* **2003**, DOI: 10.1126/science.1087139.
- (44) Walls, A. C.; Park, Y. J.; Tortorici, M. A.; Wall, A.; McGuire, A. T.; Veerler, D. *Cell* **2020**, DOI: 10.1016/j.cell.2020.02.058.
- (45) Huang, Y.; Yang, C.; feng Xu, X.; Xu, W.; wen Liu, S. Structural and functional properties of SARS-CoV-2 spike protein: potential antivirus drug development for COVID-19, 2020.
- (46) Wadman, M. *How does coronavirus kill? Clinicians trace a ferocious rampage through the body, from brain to toes. Science* **2020**, DOI: 10.1126/science.abc3208.

- (47) Hamming, I.; Timens, W.; Bulthuis, M. L.; Lely, A. T.; Navis, G. J.; van Goor, H. *Tissue distribution of ACE2 protein, the functional receptor for SARS coronavirus. A first step in understanding SARS pathogenesis. Journal of Pathology* **2004**, DOI: 10.1002/path.1570.
- (48) Charo, I. F.; Ransohoff, R. M. *The Many Roles of Chemokines and Chemokine Receptors in Inflammation. New England Journal of Medicine* **2006**, DOI: 10.1056/nejmra052723.
- (49) Wong, J. P.; Viswanathan, S.; Wang, M.; Sun, L. Q.; Clark, G. C.; D'elia, R. V. *Future Medicinal Chemistry* **2017**, DOI: 10.4155/fmc-2016-0181.
- (50) Coperchini, F.; Chiovato, L.; Croce, L.; Magri, F.; Rotondi, M. The cytokine storm in COVID-19: An overview of the involvement of the chemokine/chemokine-receptor system, 2020.
- (51) Wu, C. et al. *JAMA Internal Medicine* **2020**, DOI: 10.1001/jamainternmed.2020.0994.
- (52) Spagnolo, P.; Balestro, E.; Aliberti, S.; Cocconcelli, E.; Biondini, D.; Casa, G. D.; Sverzellati, N.; Maher, T. M. Pulmonary fibrosis secondary to COVID-19: a call to arms? 2020.
- (53) Bonaccorsi, G.; Pierri, F.; Cinelli, M.; Flori, A.; Galeazzi, A.; Porcelli, F.; Schmidt, A. L.; Valensise, C. M.; Scala, A.; Quattrocioni, W.; Pammolli, F. *Proceedings of the National Academy of Sciences of the United States of America* **2020**, DOI: 10.1073/pnas.2007658117.
- (54) WHO *Coronavirus disease (COVID-2019) situation reports. World Health Organization* **2020**.
- (55) Bernard, S.; Tilford, C.; Burn-murdoch, J. Coronavirus tracked : the latest figures as the pandemic spreads, 2020.
- (56) Max Roser Hannah Ritchie, E. O.-O.; Hasell, J. *Our World in Data* **2020**, <https://ourworldindata.org>
- (57) *Excess mortality during the Coronavirus pandemic (COVID-19) - Statistics and Research - Our World in Data.*

- (58) WIRES, N. Guayaquil, city in centre of Ecuador’s coronavirus outbreak, runs out of coffins, 2020.
- (59) Callaway, E. *The race for Coronavirus vaccines. Nature* **2020**.
- (60) Wang, Y. et al. *Remdesivir in adults with severe COVID-19: a randomised, double-blind, placebo-controlled, multicentre trial. The Lancet* **2020**, DOI: 10.1016/S0140-6736(20)31022-9.
- (61) Gautret, P. et al. *International Journal of Antimicrobial Agents* **2020**, DOI: 10.1016/j.ijantimicag.2020.105949.
- (62) Pan, H.; Peto, R.; Karim, Q. A.; Alejandria, M.; Henao-Restrepo, A. M.; García, C. H.; Kieny, M.-P.; Malekzadeh, R.; Murthy, S.; Preziosi, M.-P.; Reddy, S.; Periago, M. R.; Sathiyamoorthy, V.; Røttingen, J.-A.; Swaminathan, S. *medRxiv* **2020**.
- (63) Ngonghala, C. N.; Iboi, E.; Eikenberry, S.; Scotch, M.; MacIntyre, C. R.; Bonds, M. H.; Gumel, A. B. *Mathematical Biosciences* **2020**, DOI: 10.1016/j.mbs.2020.108364.
- (64) Brooks, B. *The Chemical Engineering Journal* **1991**, DOI: 10.1016/0300-9467(91)85016-o.
- (65) Levenspiel, O. *Chemical reaction engineering*, 1999.
- (66) Scott Fogler, H. *Chemical Engineering Science* **1987**, DOI: 10.1016/0009-2509(87)80130-6.
- (67) Jiang, S. Don’t rush to deploy COVID-19 vaccines and drugs without sufficient safety guarantees, 2020.
- (68) Vogel, G. *New blood tests for antibodies could show true scale of coronavirus pandemic. Science* **2020**, DOI: 10.1126/science.abb8028.
- (69) Stevens, H. Why outbreaks like coronavirus spread exponentially, and how to “flatten the curve”, 2020.
- (70) Li, M. Y.; Muldowney, J. S. *Mathematical Biosciences* **1995**, DOI: 10.1016/0025-5564(95)92756-5.

- (71) Bagal, D. K.; Rath, A.; Barua, A.; Patnaik, D. *Chaos, Solitons and Fractals* **2020**, DOI: 10.1016/j.chaos.2020.110154.
- (72) Andres Robalino, C. O., *COVID-19 Ecuador Database: <https://github.com/andrab/ecuacovid>*, 2020.
- (73) Ecuadorl, R. C. D., *Informes de Situacion COVID-19 Ecuador. Online resource: <https://github.com/andrab/ecuacovid/tree/master/informes/RCIV>*, 2020.
- (74) Brauer, F., *Mathematical Epidemiology*; Brauer, F., van den Driessche, P., Wu, J., Eds.; Lecture Notes in Mathematics, Vol. 1945; Springer Berlin Heidelberg: Berlin, Heidelberg, 2008, pp 19–79.
- (75) Khalili, M.; Karamouzian, M.; Nasiri, N.; Javadi, S.; Mirzazadeh, A.; Sharifi, H. Epidemiological Characteristics of COVID-19: A Systemic Review and Meta-Analysis, 2020.
- (76) Mallapaty, S. How deadly is the coronavirus? Scientists are close to an answer, 2020.
- (77) De Operaciones de Emergencia Nacional, C., *Resoluciones COE 1 de junio. Online resource: <https://www.gestionderiesgos.gob.ec/resoluciones-coe-nacional-1-de-junio-2020/>*, 2020.
- (78) Reina Ortiz, M.; Sharma, V. Modeling the COVID-19 outbreak in Ecuador: Is it the right time to lift social distancing containment measures? 2020.
- (79) INEC, *Informe de Camas y egresos hospitalarios online resource at: <https://www.ecuadorencifras.gob>* 2019.